Inorganic Chemistry

Article

pubs.acs.org/IC

Molybdenum Complex with Bulky Chelates as a Functional Model for Molybdenum Oxidases

Jana Leppin, Christoph Förster, and Katja Heinze*

Institute of Inorganic Chemistry and Analytical Chemistry, Johannes Gutenberg-University of Mainz, Duesbergweg 10−14, 55128 Mainz, Germany

Supporting Information

ABSTRACT: The novel bulky Schiff base chelate ligand [(4,5-diisopropyl-1*H*-pyrrole-2-yl)methylene]-4-(*tert*-butyl)-aniline (^{iPr2}**HL**) bearing two isopropyl groups close to the pyrrole nitrogen atom reacts with $MoCl_2(dme)O_2$ (dme = 1,2-dimethoxyethane) to give the sterically congested complex $Mo^{VI}(^{iPr2}L)_2O_2$ (^{iPr2}**1**; OC-6−4−4 configuration). In spite of the increased steric shielding of the $[MoO_2]$ unit ^{iPr2}**1** is active in oxygen-atom transfer to PMe_3 and PPh_3 to give $OPMe_3$ and $OPPh_3$, respectively. Because of the increased steric bulk of the chelate ligand, formation of dinuclear complexes $[Mo^{V}(^{iPr2}L)_2O]_2(\mu\text{-}O)$ (^{iPr2}**3**) by comportionation is effectively prevented in contrast to the highly favored formation of $[Mo^{V}(^{H2}L)_2O]_2(\mu\text{-}O)$ (^{H2}**3**) with the less bulky ligand ^{H2}**HL**. Instead, the smaller PMe_3 ligand coordinates to the resulting pentacoordinate intermediate $Mo^{IV}(^{iPr2}L)_2O$ (^{iPr2}**5**), giving the hexacoordinate complex $Mo^{IV}(^{iPr2}L)_2O(PMe_3)$ (^{iPr2}**2**) with OC-6−3−3 configuration. The larger potential ligands PPh_3 and $OPPh_3$ are only able to weakly coordinate to ^{iPr2}**5**, giving labile and sensitive $Mo^{IV}(^{iPr2}L)_2O(L)$ complexes (^{iPr2}**6**, L = PPh_3; ^{iPr2}**7**, L = $OPPh_3$). Traces of water and dioxygen in solutions of ^{iPr2}**6**/^{iPr2}**7** yield the di(μ-oxido) complex $[Mo^{V}(^{iPr2}L)O]_2(\mu\text{-}O)_2$ (^{iPr2}**4**) with reduced steric congestion due to dissociation of the bulky chelate ligands. According to electron paramagnetic resonance studies, the much more strongly bound small PMe_3 ligand in ^{iPr2}**2** can be slowly liberated by one-electron oxidation to Mo^{V}, with Ag^+ leaving a free coordination site at Mo^{V}. Hence, essentially pentacoordinate Mo^{IV} and Mo^{V} complexes are accessible as a result of the increased steric bulk.

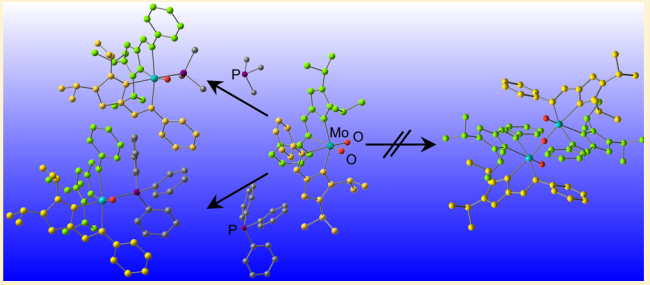

INTRODUCTION

Metal-mediated oxygen-atom transfer (OAT) is an important elementary reaction step in biology and in industrial applications.[1] In biological contexts, molybdenum enzymes[2] play a pivotal role in accomplishing this task; e.g., sulfite oxidase transforms toxic sulfite to sulfate using water as the oxygen source and two one-electron oxidants (cytochromes).[3] The model chemistry for OAT has been throroughly investigated by Holm and the groups of Basu, Enemark, Xiao, Young, and others (e.g., **A** and **B** in Chart 1).[1,4−8] Several biomimetic model complexes were introduced,[5] yet most of them allow for dinucleation in the Mo^{IV}/Mo^{V} oxidation states, which is detrimental to catalysis and which represents an abiological process.[5,6] As an exceptionally successful ligand in this respect, Trofimenko's scorpionato ligand[7] has been elegantly and extensively used by Basu, Enemark, Xiao, Young, and others in detailed studies on OAT as well as the following electron-transfer steps (Chart 1, **B**).[8] In combination with a dendritic thiolato coligand X (Chart 1, **B**), dinucleation is reported to be suppressed.[8f] The first successful forward and backward OAT involving scorpionatomolybdenum(VI/IV) complexes without intermediate formation of oxido-bridged dimers has been described by Enemark and co-workers.[8a]

Mösch-Zanetti (ketiminato and pyrazolato ancillary ligands; Chart 1, **C**)[9] and we (iminopyrrolato ancillary ligands, Chart 1, ^{H2}**HL**, **E**)[10] reported the occurrence of substrate-bound intermediates, namely, phosphane Mo^{IV} complexes, during OAT that stabilize the Mo^{IV} oxidation state.[9−12] A further strategy to prevent dinucleation by substituting a spectator oxygen atom by a bulky *tert*-butylimido ligand has been reported independently by Mösch-Zanetti and by us (Chart 1, **D** and **F**).[11,12] However, the imido complexes are prone to hydrolysis so that water cannot be used as the oxygen source.[12] Steric crowding imposed by the chelate ligand, a monodentate coligand X, or a multiply bonded spectator (imido) ligand is the most commonly employed strategy in this area.

Immobilization of OAT-active Mo^{VI} complexes on a cross-linked polymeric support proved to be a different successful strategy to suppress μ-oxido dimer formation (Chart 1, **E**; R′ = $OSi(^{i}Pr)_2$ polymer).[10a] This measure led to sustained catalysis using water as the oxygen source and ferrocenium ions as terminal oxidants.[10a] Functionalized chelate ligands and derived $Mo^{VI/IV}$ complexes with built-in ferrocenium oxidants to

Received: July 23, 2014
Published: November 13, 2014

   dx.doi.org/10.1021/ic501751p | *Inorg. Chem.* 2014, 53, 12416−12427

Chart 1. MoO_2 Complexes Relevant to OAT by Holm (A) and Basu/Enemark/Xiao/Young (B), MoO_2 and MoO(N*t*Bu) Complexes by Mösch-Zanetti (C and D) and Heinze (E and F), Immobilized MoO_2 Complexes by Heinze (E), and MoO_2 Complexes with Built-In Redox Sites (G)

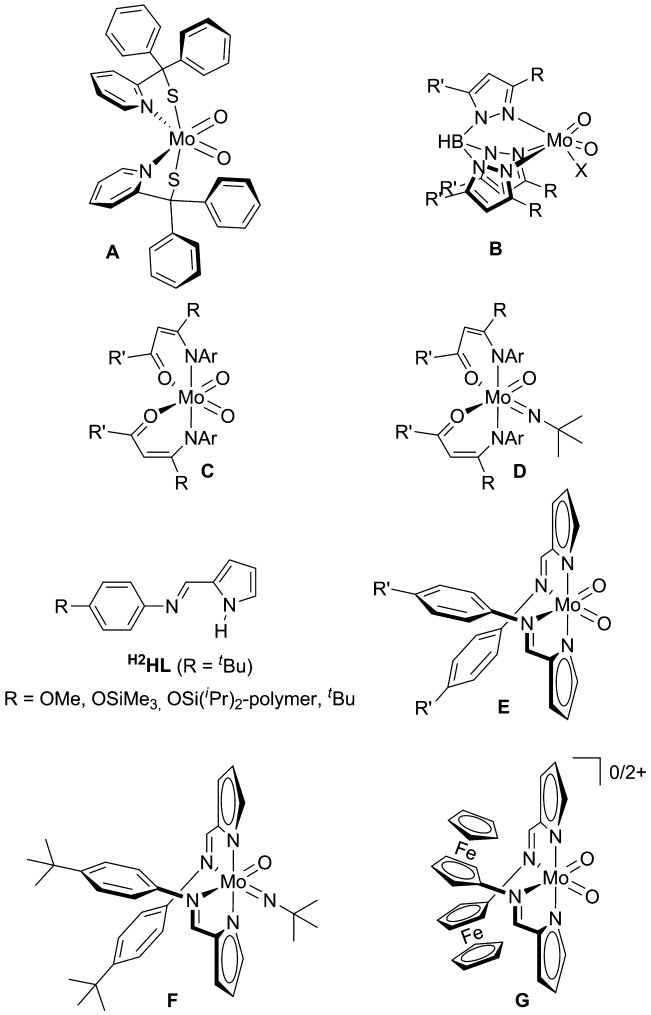

facilitate electron transfer between Mo^{IV} and Fe^{III} have been reported recently by our group (Chart 1, **G**).[13]

Here we employ steric crowding imposed by the chelate ligand to suppress dinucleation in $Mo^{IV/V}O$ complexes of the Schiff base ligand ^{R2}**HL**, namely, protection of the active site by sterically demanding groups at the chelate ligand close to the pyrrole nitrogen donor atom similar to Holm's pyridyl thiolato complexes (Chart 1, **A**). The impact of the increased steric bulk on the reactivity, (stereo)selectivity, and stability of $Mo^{VI/V/IV}$ complexes will be disclosed in this study.

EXPERIMENTAL SECTION

General Procedures. All reactions involving molybdenum complexes were performed under an inert atmosphere (Schlenk techniques, glovebox). Tetrahydrofuran (THF) was distilled from potassium, dichloromethane, diethyl ether, and petroleum ether 40–60 °C from calcium hydride. $MoCl_2(dme)O_2$ (dme = 1,2-dimethoxyethane)[14] and $[Mo^V(^{H2}L)_2O]_2(\mu\text{-}O)$ (^{H2}**3**)[10,12] were prepared according to literature procedures. All other reagents were used as received from commercial suppliers (Acros, Sigma-Aldrich). NMR spectra were recorded on a Bruker Avance DRX 400 spectrometer at 400.31 MHz (^{1}H), 100.66 MHz (^{13}C{^{1}H}), 162.05 MHz (^{31}P{^{1}H}), and 40.56 MHz (^{15}N). All resonances are reported in ppm versus the solvent signal as the internal standard [THF-d_8 (^{1}H, δ 1.73, 3.58; ^{13}C, δ 25.37, 67.57); $CDCl_3$ (^{1}H, δ 7.26; ^{13}C, δ 77.16); C_6D_6 (^{1}H, δ 7.16; ^{13}C, δ 128.06)] versus external H_3PO_4 (85%; ^{31}P, δ 0) and external CH_3NO_2 (90% in $CDCl_3$; ^{15}N, δ 380.23). ^{15}N data are reported versus liquid NH_3 as the reference (δ 0). Diffusion-ordered spectroscopy (DOSY) experiments were performed in THF-d_8 (log D/m^2 s^{-1} = −8.6) or C_6D_6 (log D/m^2 s^{-1} = −8.7) at 25 °C.[15] IR spectra were recorded with a BioRad Excalibur FTS 3100 spectrometer as CsI disks. Electrochemical experiments were carried out on a BioLogic SP-50 voltammetric analyzer using platinum wires as the counter and working electrodes and 0.01 M $Ag/AgNO_3$ as the reference electrode. The cyclic voltammetry (CV) measurements were carried out at scan rates of 50–100 mV s^{-1} using 0.1 M $[^nBu_4N][B(C_6F_5)_4]$ as the supporting electrolyte in THF. Potentials were referenced to the ferrocene/ferrocenium couple ($E_{1/2}$ = 220 ± 5 mV under the experimental conditions). UV/vis/near-IR (NIR) spectra were recorded on a Varian Cary 5000 spectrometer using 1.0 cm cells (Hellma, Suprasil). Field-desorption mass spectrometry (FD-MS) spectra were recorded on a FD Finnigan MAT95 spectrometer. Electrospray ionization mass spectrometry (ESI-MS) spectra were recorded on a Micromass Q-TOF-Ultima spectrometer. X-band continuous-wave electron paramagnetic resonance (EPR) spectra were recorded on a Magnettech MS 300 spectrometer with a Hewlett-Packard 5340A frequency counter at a microwave frequency of 9.39 GHz in solution (298 K). Mn^{2+} in ZnS was used as the external standard. Simulations were performed with the program package *EasySpin*.[16] Elemental analyses were performed by the Microanalytical Laboratory of the Chemical Institutes of the University of Mainz.

Crystal Structure Determination. Intensity data were collected using a Bruker AXS Smart1000 CCD diffractometer equipped with an APEX II detector and an Oxford cooling system using Mo Kα radiation (λ = 0.71073 Å) at 173(2) K and corrected for absorption and other effects. The diffraction frames were integrated using the *SAINT* package, and most were corrected for absorption with *MULABS*.[17,18] The structures were solved by direct or Patterson methods and refined by the full-matrix method based on F^2 using the *SHELXTL* software package.[19,20] All non-hydrogen atoms were refined anisotropically, while the positions of all hydrogen atoms were generated with appropriate geometric constraints and allowed to ride on their respective parent atoms with fixed isotropic thermal parameters. Plots with thermal ellipsoids are given in the Supporting Information (SI; Figures S1–S4). Crystallographic data (excluding structure factors) for the structures reported in this paper have been deposited with the Cambridge Crystallographic Data Centre as CCDC 965852 (1*H*-pyrrole-4,5-diisopropyl-2-carbaldehyde), 965850 (^{iPr2}**1**), 965851 (^{H2}**3**), and 984218 (^{iPr2}**4**). Copies of the data can be obtained free of charge upon application to CCDC, 12 Union Road, Cambridge CB2 1EZ, U.K. [fax (044) 1223-336-033; e-mail deposit@ccdc.cam.ac.uk].

Crystallographic data of 1*H*-pyrrole-4,5-diisopropyl-2-carbaldehyde: $C_{11}H_{17}NO$ (179.26); orthorhombic; *Pbca*; a = 7.339(3) Å, b = 13.480(5) Å, c = 22.404(12) Å, V = 2216.4(17) Å^3; Z = 8; density, calcd = 1.074 g cm^{-3}, μ = 0.068 mm^{-1}; F(000) = 784.0; crystal size 0.40 × 0.20 × 0.08 mm; θ = 1.82–28.05°; $-9 \le h \le 9$, $-17 \le k \le 17$, $-29 \le l \le 13$; reflns collected = 14151; reflns unique = 2679 [R(int) = 0.1155]; completeness to θ = 28.05° = 99.8%; semiempirical absorption correction from equivalents; max and min transmission 0.995 and 0.973; data 2679; restraints 0, parameters 122; GOF on F^2 = 0.755; final R indices [$I > 2\sigma(I)$] R1 = 0.0499, wR2 = 0.0947; R indices (all data) R1 = 0.1532, wR2 = 0.1189; largest difference peak and hole 0.282 and −0.231 e Å^{-3}. The molecule contains no heavy atoms, and the investigated crystal was a very thin plate, resulting in a low ratio of observed to unique reflections. It was not possible to obtain crystals of higher quality suitable for X-ray analysis.

Crystallographic data of ^{iPr2}**1**: $C_{42}H_{58}MoN_4O_2$ (746.86); monoclinic; $P2_1/c$; a = 18.9095(10) Å, b = 11.1731(5) Å, c = 21.0776(10) Å, β = 114.391(5)°, V = 4055.8(3) Å^3; Z = 4; density, calcd = 1.223 g cm^{-3}, μ = 0.361 mm^{-1}; F(000) = 1584; crystal size 0.30 × 0.09 × 0.06 mm; θ = 2.37–28.01°; $-24 \le h \le 23$, $-14 \le k \le 14$, $-27 \le l \le 26$; reflns collected = 38051; reflns unique = 9766 [R(int) = 0.0779];

dx.doi.org/10.1021/ic501751p | *Inorg. Chem.* 2014, 53, 12416–12427

completeness to θ = 28.01° = 99.6%; semiempirical absorption correction from equivalents; max and min transmission 0.979 and 0.899; data 9766; restraints 0, parameters 442; GOF on F^2 = 0.840; final R indices [$I > 2\sigma(I)$] R1 = 0.0365, wR2 = 0.0652; R indices (all data) R1 = 0.0720, wR2 = 0.0716; largest difference peak and hole 0.428 and −0.680 e Å^{-3}. The large and highly anisotropic temperature factors for the atoms of the *i*Pr and *t*Bu groups indicate nonresolved rotational disorder as is typical for these substituents. It was not possible to obtain crystals of higher quality suitable for X-ray analysis.

Crystallographic data of ^{H2}**3**: $C_{60}H_{68}Mo_2N_8O_3$ (1141.10); triclinic; $P\bar{1}$; a = 9.7310(12) Å, b = 11.4519(12) Å, c = 13.2828(14) Å, α = 101.136(4)°, β = 95.064(3)°, γ = 99.356(3)°, V = 1422.0(3) Å^3; Z = 1; density, calcd = 1.332 g cm^{-3}, μ = 0.491 mm^{-1}; F(000) = 592; crystal size 0.42 × 0.37 × 0.25 mm; θ = 2.49−27.00°; $-12 \le h \le 12$, $-14 \le k \le 14$, $-16 \le l \le 16$; reflns collected = 14007; reflns unique = 6161 [R(int) = 0.0535]; completeness to θ = 27.00° = 99.2%; semiempirical absorption correction from equivalents; max and min transmission 0.887 and 0.820; data 6161; restraints 9, parameters 336; GOF on F^2 = 1.011; final R indices [$I > 2\sigma(I)$] R1 = 0.0489, wR2 = 0.1195; R indices (all data) R1 = 0.0700, wR2 = 0.1290; largest difference peak and hole 1.126 and −0.809 e Å^{-3}. The large and highly anisotropic temperature factors for atoms of the *t*Bu groups indicate nonresolved rotational disorder asis typical for these substituents. One *t*Bu group has been refined isotropically with a second occupied site using SAME and SADI restraints [ratio 0.790(37):0.210(37)]. It was not possible to obtain crystals of higher quality suitable for X-ray analysis.

Crystallographic data of ^{iPr2}**4**·THF: $C_{46}H_{66}Mo_2N_4O_5$ (946.91); orthorhombic; $P2_12_12$; a = 12.4578(11) Å, b = 31.036(3) Å, c = 12.3794(11) Å, V = 4786.3(7) Å^3; Z = 4; density, calcd = 1.314 g cm^{-3}, μ = 0.569 mm^{-1}; F(000) = 1976; crystal size 0.11 × 0.02 × 0.01 mm; θ = 2.32−27.90°; $-16 \le h \le 16$, $-40 \le k \le 40$, $-16 \le l \le 16$; reflns collected = 58998; reflns unique = 11416 [R(int) = 0.2608]; completeness to θ = 27.90° = 99.8%; semiempirical absorption correction from equivalents; max and min transmission 0.994 and 0.940; data 11416; restraints 3, parameters 516; GOF on F^2 = 0.733; final R indices [$I > 2\sigma(I)$] R1 = 0.0538, wR2 = 0.0593; R indices (all data) R1 = 0.2010, wR2 = 0.0810; largest difference peak and hole 0.475 and −0.746 e Å^{-3}; absolute structure parameter 0.39(5). The large and highly anisotropic temperature factors for atoms of the *i*Pr and *t*Bu groups and the THF molecules indicate nonresolved rotational disorder typical for these entities. The investigated crystal was a very thin plate, resulting in a low ratio of observed to unique reflections. It was not possible to obtain crystals of higher quality suitable for X-ray analysis.

Density Functional Theory (DFT) Calculations. DFT calculations were carried out with the *Gaussian09/DFT*[21] series of programs. The B3LYP formulation of DFT was used, employing the LANL2DZ basis set supplemented by d-type polarization functions[22a] on nitrogen (ζ = 0.864), oxygen (ζ = 1.154), and phosphorus (ζ = 0.340). All structures were characterized as minima by frequency analysis (N_{imag} = 0). No symmetry constraints were imposed on the molecules. Solvent modeling was done by employing the integral equation formalism polarizable continuum model (IEFPCM, THF). The modeled complexes were slightly simplified by replacing the *t*Bu group of the chelate ligands with a hydrogen atom. For calculations of the EPR parameters, the EPR-II basis set[22b] was used for carbon, hydrogen, nitrogen, and oxygen, the WTBS basis set[22c] for molybdenum, and 6-311++G(2d,2p) for phosphorus.

Synthesis of 1*H*-Pyrrole-4,5-diisopropyl-2-carbaldehyde. To a mixture of *N*,*N*-dimethylformamide (9.3 mL, 8.8 g, 120 mmol) and 1,2-dichloroethane (45 mL) was added oxalyl chloride (10.3 mL, 15.2 g, 120 mmol) dropwise within 15 min under cooling to 0 °C. After the suspension was stirred for 15 min at room temperature, pyrrole (8.3 mL, 8.1 g, 120 mmol) dissolved in 1,2-dichloroethane (50 mL) was added dropwise under cooling to 0 °C. After the clear solution was stirred for 15 min at room temperature, isopropyl chloride (16.4 mL, 14.1 g, 180 mmol) was added. Under an inert atmosphere, finely ground and dried aluminum chloride (24 g, 180 mmol) was added in small portions, and the mixture was stirred for 2.5 h at room temperature. After the addition of ice water (200 mL), the organic phase was extracted twice with water (2 × 100 mL). The aqueous phase was neutralized with KOH until pH 9, giving a white precipitate, which was dissolved by adding concentrated HCl_{aq} (ca. pH 1). This mixture was extracted with ethyl acetate (3 × 200 mL). The combined organic phases were dried over $MgSO_4$, and the solvent was removed under reduced pressure. The resulting dark oil crystallized upon standing, and the resulting colorless crystals were recrystallized from ethyl acetate. Yield: 14% (1.04 g, 5.8 mmol). Mp: 122 °C. Elem anal. Calcd for $C_{11}H_{17}NO$ (179.26): C, 73.70; H, 9.56; N, 7.81. Found: C, 73.40; H, 9.63; N, 8.09. FD-MS: m/z 179.6 (100%; [M]$^+$). IR (CsI): $\tilde{\nu}$ 3267 (m, NH), 2959 (m, CH), 1651 (br, CO), 1255 (m), 790 (m) cm^{-1}. ^{1}H NMR ($CDCl_3$): δ 9.32 (s, 1H, H^7), 9.11 (br s, 1H, NH), 6.80 (d, $^4J_{HH}$ = 2.5 Hz, 1H, H^9; correlation to NH observed in the TOCSY spectrum), 3.11 (sept, $^3J_{HH}$ = 7.0 Hz, 1H, H^{14}), 2.85 (sept, $^3J_{HH}$ = 6.8 Hz, 1H, H^{16}), 1.28 (d, $^3J_{HH}$ = 7.0 Hz, 6H, H^{15}), 1.20 (d, $^3J_{HH}$ = 6.9 Hz, 6H, H^{16}). ^{13}C{^{1}H} NMR ($CDCl_3$): δ 177.9 (s, C^7), 143.6 (s, C^{11}), 130.7 (s, C^8), 130.1 (s, C^{10}), 119.5 (s, C^9), 25.6 (s, C^{14}), 25.0 (s, C^{16}), 24.5 (s, C^{17}), 22.4 (s, C^{15}). ^{15}N{^{1}H} NMR ($CDCl_3$): δ 139.9 (s, N^p). UV/vis [THF; λ_{max}, nm (ε, M^{-1} cm^{-1})]: 251 (3225), 305 (12165).

Synthesis of [(4,5-Diisopropyl-1*H*-pyrrole-2-yl)methylene]-4-(*tert*-butyl)aniline (^{iPr2}HL). 1*H*-Pyrrole-4,5-diisopropyl-2-carbaldehyde (1 g, 5.6 mmol) was dissolved in toluene (80 mL), and 4-*tert*-butylaniline (0.9 mL, 836 mg, 5.6 mmol) was added together with some molecular sieve (3 Å). After heating under reflux for 16 h, the mixture was filtered. The solvent was removed under reduced pressure, and a viscous oil was obtained, which crystallized slowly to a yellow solid upon standing. Yield: 80% (1.4 g, 4.4 mmol). Mp: 78 °C. Elem anal. Calcd for $C_{21}H_{30}N_2 \cdot {}^1/_3H_2O$ (310.48): C, 79.70; H, 9.77; N, 8.85. Found: C, 79.60; H, 9.27; N, 8.86. FD-MS: m/z 310.5 (100%; [M]$^+$). IR (CsI): $\tilde{\nu}$ 3260 (br, NH), 3028 (w, CH), 2957 (m), 2928 (w), 2866 (w, CH), 1622 (m), 1594 (m), 1562 (m), 1263 (m), 1163 (m), 1140 (m), 831 (m) cm^{-1}. ^{1}H NMR (THF-d_8): δ 10.25 (s, 1H, NH), 8.09 (s, 1H, H^7), 7.33 (d, $^3J_{HH}$ = 8.6 Hz, 2H, H^{3,5}), 7.02 (d, $^3J_{HH}$ = 8.6 Hz, 2H, H^{2,6}), 6.44 (s, 1H, H^9), 3.12 (sept, $^3J_{HH}$ = 7.1 Hz, 1H, H^{14}), 2.89 (sept, $^3J_{HH}$ = 6.9 Hz, 1H, H^{16}), 1.32 (s, 9H, H^{13}), 1.31 (d, $^3J_{HH}$ = 7.2 Hz, 6H, H^{15}), 1.19 (d, $^3J_{HH}$ = 6.9 Hz, 6H, H^{17}). ^{13}C{^{1}H} NMR (THF-d_8): δ 151.6 (s, C^1), 149.5 (s, C^7), 148.0 (s, C^4), 140.2 (s, C^{11}), 130.2 (s, C^8), 128.4 (s, C^{10}), 126.5 (s, C^{3,5}), 121.0 (s, C^{2,6}), 115.0 (s, C^9), 35.0 (s, C^{12}), 31.9 (s, C^{13}), 26.7 (s, C^{14}), 26.0 (s, C^{16}), 24.9 (s, C^{17}), 22.9 (s, C^{15}). ^{15}N{^{1}H} NMR (THF-d_8): δ 292.7 (s, N^i), 138.6 (s, N^p). DOSY (THF-d_8): log D/m^2 s^{-1} = −9.0. DOSY (C_6D_6): log D/m^2 s^{-1} = −9.1. UV/vis [THF; λ_{max}, nm (ε, M^{-1} cm^{-1})]: 343 (24000).

Synthesis of ^{iPr2}1. Potassium bis(trimethylsilyl)amide (238 mg, 1.193 mmol) dissolved in THF (3 mL) was added to a solution of ligand ^{iPr2}HL (370 mg, 1.193 mmol) in THF (10 mL). The yellow mixture was stirred for 30 min at room temperature. $MoCl_2(dme)O_2$[14] (172 mg, 0.596 mmol) dissolved in THF (2 mL) was added to the yellow solution, which turned red. After heating to reflux for 5.5 h, the solvent was removed under reduced pressure. To remove bis(trimethylsilyl)amine, the powder was dried at 60 °C under reduced pressure for 12 h. The residue was dissolved in diethyl ether (10 mL), and KCl was removed by filtration. The solvent was removed under reduced pressure, and the remaining red solid was recrystallized from petroleum ether 40−60 °C. Yield: 70% (625 mg, 0.84 mmol). Mp: 204 °C. Elem anal. Calcd for $C_{42}H_{58}N_4MoO_2$ (748.36): C, 67.54; H, 7.83; N, 7.50. Found: C, 67.26; H, 7.90; N, 8.29. FD-MS: m/z 748.4 (100%; [M]$^+$). IR (CsI): $\tilde{\nu}$2963 (m, CH), 1611 (m), 1588 (s), 1531 (m), 1163 (m), 932 (m, MoO), 900 (m, MoO) cm^{-1}. ^{1}H NMR (THF-d_8): δ 7.77 (s, 1H, H^7), 7.16 (d, $^3J_{HH}$ = 8.4 Hz, 2H, H^{3,5}), 6.85 (d, $^3J_{HH}$ = 8.4 Hz, 2H, H^{2,6}), 6.40 (s, 1H, H^9), 3.65 (pseudo sept, $^3J_{HH}$ = 7.2 Hz, 1H, H^{14}), 3.06 (pseudo sept, $^3J_{HH}$ = 6.8 Hz, 1H, H^{16}), 1.37 (d, $^3J_{HH}$ = 7.2 Hz, 6H, H$^{15\prime}$), 1.32 (d, $^3J_{HH}$ = 7.0 Hz, 6H, H^{15}), 1.26 (s, 9H, H^{13}), 1.11 (d, $^3J_{HH}$ = 6.4 Hz, 6H, H$^{17\prime}$), 1.10 (d, $^3J_{HH}$ = 6.4 Hz, 6H, H^{17}). ^{13}C{^{1}H} NMR (THF-d_8): δ 157.1 (s, C^7), 154.8 (s, C^{11}), 148.6 (s, C^4), 148.2 (s, C^1), 138.1 (s, C^8), 135.1 (s, C^{10}), 126.0 (s, C^{3,5}), 122.4 (s, C^{2,6}), 120.3 (s, C^9), 34.8 (s, C^{12}), 31.8 (s, C^{13}), 29.3 (s, C^{14}), 26.5 (s, C^{16}), 25.5 (s, C^{17}), 25.1 (s, C$^{17\prime}$), 23.5 (s, C^{15}), 21.7 (s, C$^{15\prime}$). ^{15}N{^{1}H} NMR (THF-d_8): δ 241.1 (s, N^i), 214.9 (s, N^p). DOSY

(THF-d_8): log D/m^2 s^{-1} = −9.0. DOSY (C_6D_6): log D/m^2 s^{-1} = −9.2. UV/vis [THF; λ_{max}, nm (ε, M^{-1} cm^{-1})]: 322 (42780), 447 (6245). CV (THF): E_p = −1.78 V (qrev; oxidative follow-up wave at E_p = −1.37 V).

One-Electron Reduction of ^{iPr2}1. To decamethylcobaltocene $CoCp^*_2$ (2.2 mg, 6.7 × 10^{-3} mmol) suspended in CH_2Cl_2 (0.5 mL) was added ^{iPr2}**1** (5 mg, 6.7 × 10^{-3} mmol) dissolved in CH_2Cl_2 (1 mL). The solution was stirred for 5 h at room temperature and turned orange. After removal of the solvent under reduced pressure, an orange powder was obtained. Elem anal. Calcd for $C_{62}H_{90}CoMoN_4O_2$ (1078.30). ESI$^+$-MS: m/z 329.1 (100%; [$CoCp^*_2$]$^+$). IR (CsI): $\tilde{\nu}$ 2962 (m, CH), 1618 (m), 1587 (s), 1482 (m, Cp*), 1265 (m), 1167 (m), 1103 (m, Cp*), 1050 (m, Cp*), 1024 (m, Cp*), 874 (m, MoO), 801 (m, MoO) cm^{-1}. EPR (298 K, CH_2Cl_2): g = 1.9439, A($^{95/97}$Mo) = 40 × 10^{-4} cm^{-1} (44 G). EPR (77 K, CH_2Cl_2): $g_{1,2,3}$ = 1.9664, 1.9450, 1.9248. UV/vis [CH_2Cl_2; λ_{max}, nm (ε, M^{-1} cm^{-1})]: 296 (47855), 344 (32810), 429 (6640).

Synthesis of ^{iPr2}2. The dioxido complex ^{iPr2}**1** (50 mg, 0.069 mmol) was dissolved in THF (3 mL), and trimethylphosphane (1 M in THF, 1.02 mL, 1.02 mmol) was added. After stirring for 3 days at room temperature, volatiles were removed under reduced pressure to give a yellow-green powder. Attempts to completely remove phosphane oxide by recrystallization from petroleum ether, THF, or toluene failed (ca. 0.16 equiv by ^{1}H NMR). Yield: 40 mg (0.047 mmol, 68% calculated including 0.16 equiv of $OPPh_3$). Elem anal. Calcd for $C_{45}H_{67}N_4MoOP$ (806.97). FD-MS: m/z 806.5 (16%; [M]$^+$). IR (CsI): $\tilde{\nu}$ 2963 (s, CH), 1608 (m), 1580 (s), 1514 (m), 1163 (m), 1101 (m), 946 (m, MoO), 800 (br) cm^{-1}. ^{1}H NMR (THF-d_8): δ 7.93 (s, 1H, H^{7a}), 7.73 (d, $^4J_{PH}$ = 0.96 Hz, 1H, H^{7b}), 7.62 (d, $^3J_{HH}$ = 8.6 Hz, 2H, H^{2b,6b}), 7.45 (d, $^3J_{HH}$ = 8.6 Hz, 2H, H^{3a,5a}), 7.38 (d, $^3J_{HH}$ = 8.6 Hz, 2H, H^{3b,5b}), 7.28 (d, $^3J_{HH}$ = 8.6 Hz, 2H, H^{2a,6a}), 6.91 (s, 1H, H^{9a}), 6.30 (br s, $^5J_{PH}$ < 1 Hz, 1H, H^{9b}), 3.30 (pseudo sept, $^3J_{HH}$ = 7.2 Hz, 1H, H^{14a}), 3.00 (pseudo sept, $^3J_{HH}$ = 6.8 Hz, 1H, H^{16a}), 2.81 (pseudo sept, $^3J_{HH}$ = 6.8 Hz, 1H, H^{16b}), 2.60 (pseudo sept, $^3J_{HH}$ = 7.2 Hz, 1H, H^{14b}), 1.35 (s, 18H, H^{13a,13b}), 1.19 (d, $^3J_{HH}$ = 7.1 Hz, 3H, H^{17a}), 1.16 (d, $^3J_{HH}$ = 7.7 Hz, 3H, H^{15a}), 1.14 (d, $^3J_{HH}$ = 7.7 Hz, 1H, H^{15b}), 1.12 (d, $^3J_{HH}$ = 7.1 Hz, 3H, H$^{17a\prime}$), 1.04 (d, $^3J_{HH}$ = 6.7 Hz, 1H, H^{17b}), 1.01 (d, $^3J_{HH}$ = 6.8 Hz, 1H, H$^{17b\prime}$), 0.83 (d, $^3J_{HH}$ = 7.1 Hz, 1H, H$^{15b\prime}$), 0.73 (d, $^3J_{HH}$ = 7.1 Hz, 1H, H$^{15a\prime}$), 0.71 (d, $^2J_{PH}$ = 8.4 Hz, 9H, PMe_3). ^{1}H NMR (residual $OPMe_3$): δ 1.34 (d, $^3J_{HH}$ = 13.0 Hz, $OPMe_3$). ^{13}C{^{1}H} NMR (THF-d_8): δ 164.6 (s, C^{11a}), 157.8 (s, C^{11b}), 157.6 (s, C^{7a}), 156.2 (s, C^{1a}), 153.0 (s, C^{1b}), 149.2 (s, C^{7b}), 148.0 (s, C^{4b}), 149.3 (s, C^{4a}), 140.8 (s, C^{8a}), 138.6 (s, C^{8b}), 136.9 (s, C^{10a}), 134.1 (s, C^{10b}), 126.5 (s, C^{3a,5a}), 126.0 (s, C^{3b,5b}), 123.6 (s, C$^{2a,6a/2b,6b}$), 120.5 (s, C^{9a}), 115.4 (s, C^{9b}), 35.2 (s, C^{12a,12b}), 31.9 (s, C^{13a,13b}), 31.2 (s, C^{14b}), 30.8 (s, C^{14a}), 26.7 (s, C^{16a,16b}), 26.1 (s, C$^{17b\prime}$), 25.5 (s, C^{17a}), 25.5 (s, C^{17b}), 25.4 (s, C$^{17a\prime}$), 24.3 (s, C^{15b}), 23.0 (s, C$^{15b\prime}$), 22.6 (s, C^{15a}), 22.5 (s, C$^{15a\prime}$), 18.3 (d, $^3J_{HH}$ = 69.0 Hz, PMe_3). ^{15}N{^{1}H} NMR (THF-d_8): δ 226.9 (s, N^{pb}), 225.1 (s, N^{ib}), 223.9 (s, N^{pa}), 208.4 (s, N^{ia}). ^{31}P{^{1}H} NMR: δ −1.70. DOSY (THF-d_8): log D/m^2 s^{-1} = −9.1. DOSY (C_6D_6): log D/m^2 s^{-1} = −9.1. UV/vis [THF; λ_{max}, nm (ε, M^{-1} cm^{-1})]: 345 (28450), 425 (16250), 505 (sh, 2120), 685 (230). CV (THF): $E_{1/2}$ = −0.40 V.

OAT with PPh_3. The dioxido complex ^{iPr2}**1** (5.86 mg, 0.0078 mmol) was dissolved in C_6D_6 (0.6 mL), and triphenylphosphane (3.85 mg, 0.015 mmol, 1.92 equiv) was added. In other NMR experiments 5 equiv of PPh_3 was used. ^{1}H and ^{31}P NMR spectra were recorded during the following days. At the final stage of the reaction, 2D NMR spectra (^{1}H^{1}H COSY, ^{1}H^{1}H NOESY, ^{1}H^{13}C HSQC, ^{1}H^{13}C HMBC, ^{1}H^{31}P HMBC, DOSY) of the reaction mixture were acquired. For UV/vis experiments, the dioxido complex ^{iPr2}**1** dissolved in petroleum ether 40−60 °C (5.4 × 10^{-5} M, 3 mL) and triphenylphosphane dissolved in petroleum ether 40−60 °C (1.9 × 10^{-4} M, 1.7 mL) were combined (1:2 equiv). UV/vis spectra were recorded during the following 35 h. In one experiment conducted in THF, a few crystals of the decomposed complex ^{iPr2}**4**·THF separated from the solution upon standing for several weeks. ^{iPr2}**4**. FD-MS: m/z 875.2 (100%; [M]$^+$). IR (CsI): $\tilde{\nu}$ 2966 (m, CH), 1585 (m), 1261 (s), 1099 (s, residual PO), 1020 (s, residual $OPPh_3$), 970 (m, MoO), 953 (sh, MoO), 800 (br), 743 (m), 698 (m, MoO_2Mo), 692 (sh, MoO_2Mo) cm^{-1}. ^{1}H NMR (THF-d_8): δ 8.23 (s, 1H, H^7), 7.58 (d, $^3J_{HH}$ = 8.5 Hz, 2H, H^{2,6}), 7.52 (d, $^3J_{HH}$ = 8.6 Hz, 2H, H^{3,5}), 6.84 (s, 1H, H^9), 4.30 (pseudo sept, $^3J_{HH}$ = 7.2 Hz, 1H, H^{14}), 3.03 (pseudo sept, $^3J_{HH}$ = 6.6 Hz, 1H, H^{16}), 1.43 (s, 9H, H^{13}), 1.28 (d, $^3J_{HH}$ = 7.2 Hz, 3H, H$^{15\prime}$), 1.22 (d, $^3J_{HH}$ = 6.6 Hz, 3H, H^{17}), 1.07 (d, $^3J_{HH}$ = 6.6 Hz, 3H, H$^{17\prime}$), 0.99 (d, $^3J_{HH}$ = 7.2 Hz, 3H, H^{15}). ^{13}C{^{1}H} NMR (THF-d_8): δ 163.6 (s, C^{11}), 157.2 (s, C^7), 149.1 (s, C^4), 148.8 (s, C^1), 138.6 (s, C^8), 137.6 (s, C^{10}), 126.5 (s, C^{3,5}), 123.6 (s, C^{2,6}), 122.7 (s, C^9), 35.2 (s, C^{12}), 31.9 (s, C^{13}), 30.7 (s, C^{14}), 26.5 (s, C^{16}), 25.2 (s, C$^{17\prime}$), 24.9 (s, C^{17}), 22.7 (s, C^{15}), 21.8 (s, C$^{15\prime}$). ^{15}N{^{1}H} NMR (THF-d_8): δ 211.6 (s, N^i), 211.4 (s, N^p). DOSY (THF-d_8): log D/m^2 s^{-1} = −9.1. DOSY (C_6D_6): log D/m^2 s^{-1} = −9.2. UV/vis [THF; λ_{max}, nm (ε, M^{-1} cm^{-1})]: 308 (28240), 450 (22720).

Final major product in solution, slow species. ^{1}H NMR (C_6D_6): δ 7.32 (d, $^3J_{HH}$ = 8.4 Hz, 2H, H^{3b,5b}), 6.95 (d, $^3J_{HH}$ = 8.4 Hz, 2H, H^{3a,5a}), 6.95 (s, 1H, H^{7b}), 6.90 (s, 1H, H^{7a}), 6.77 (s, 1H, H^{9b}), 6.53 (s, 1H H^{9a}), 6.25 (d, $^3J_{HH}$ = 8.3 Hz, 2H, H^{2b,6b}), 6.18 (d, $^3J_{HH}$ = 8.4 Hz, 2H, H^{2a,6a}), 5.09 (pseudo sept, $^3J_{HH}$ = 7.2 Hz, 1H, H^{14b}), 3.45 (pseudo sept, $^3J_{HH}$ = 6.6 Hz, 1H, H^{16b}), 3.10 (pseudo sept, $^3J_{HH}$ = 6.6 Hz, 1H, H^{16a}), 2.33 (pseudo sept, $^3J_{HH}$ = 7.2 Hz, 1H, H^{14a}), 1.85 (d, $^3J_{HH}$ = 7.0 Hz, 3H, H^{15b}), 1.71 (d, $^3J_{HH}$ = 7.0 Hz, 3H, H$^{15b\prime}$), 1.43 (d, $^3J_{HH}$ = 7.1 Hz, 3H, H^{15a}), 1.42 (d, $^3J_{HH}$ = 7.0 Hz, 3H, H^{17b}), 1.42 (d, $^3J_{HH}$ = 7.0 Hz, 3H, H$^{17b\prime}$), 1.40 (s, 9H, H^{13b}), 1.29 (d, $^3J_{HH}$ = 7.0 Hz, 3H, H^{17a}), 1.26 (d, $^3J_{HH}$ = 6.8 Hz, 3H, H$^{15a\prime}$), 1.20 (d, $^3J_{HH}$ = 6.8 Hz, 3H, H$^{17a\prime}$), 0.99 (s, 9H, H^{13a}); the resonances of coordinated PPh_3/$OPPh_3$ are indistinguishable from those of free PPh_3/$OPPh_3$. ^{13}C NMR (C_6D_6): δ 163.5 (s, C^{11a}), 155.50 (s, C^{11b}), 151.9 (s, C^{1a}), 149.1 (s, C^{1b}), 147.8 (s, C^{4b}), 146.6 (s, C^{4a}), 136.9 (s, C^{10b}), 136.9 (s, C^{8a}), 135.8 (s, C^{8b}), 138.3 (s, C^{10a}), 159.1 (s, C^{7a}), 156.8 (s, C^{7b}), 125.9 (s, C^{3a,5a}) 124.9 (s, C^{3b,5b}), 124.0 (s, C^{2b,6b}), 124.1 (s, C^{2a,6a}), 122.0 (s, C^{9a}), 119.6 (s, C^{9b}), 34.3 (s, C^{12b}), 34.2 (s, C^{12a}), 30.4 (s, C^{14b}), 31.5 (s, C^{13b}), 31.2 (s, C^{13a}), 29.2 (s, C^{14a}), 26.24 (s, C^{16a}), 26.1 (s, C^{16b}), 25.8 (s, C$^{17b,17b\prime}$), 25.8 (s, C^{17a}), 24.8 (s, C$^{17a\prime}$), 23.8 (s C$^{15b\prime}$), 23.5 (s, C$^{15a\prime}$), 23.4 (s, C^{15a}), 23.3 (s C^{15b}); the resonances of coordinated PPh_3/$OPPh_3$ are indistinguishable from those of free PPh_3/$OPPh_3$. DOSY (C_6D_6): log D/m^2 s^{-1} = −9.3. UV/vis (petroleum ether 40−60 °C; λ_{max}, nm): 329, 456.

One-Electron Oxidation of ^{iPr2}2. To ^{iPr2}**2** (2.5 mg, 0.003 mmol) dissolved in THF (1 mL) was added $AgSbF_6$ (1.1 mg, 0.003 mmol) in THF (0.5 mL). The solution was filtered into an EPR tube. EPR (295 K, THF): g = 1.9667, A($^{95/97}$Mo) = 31 × 10^{-4} cm^{-1} (33.5 G), A(^{31}P) = 16.5 × 10^{-4} cm^{-1} (18.0 G) [70%]; g = 1.9455, A($^{95/97}$Mo) = 42.5 × 10^{-4} cm^{-1} (47.0 G) [30%]. ESI$^+$-MS: m/z 824.5 (58%; [^{iPr2}**2** + O]$^+$), 808.5 (74%; [^{iPr2}**2**]$^+$), 732.4 (100%; [^{iPr2}**2** − PMe_3]$^+$). IR (CsI): $\tilde{\nu}$ 2963 (s, CH), 1660 (m), 1586 (s), 1511 (m), 1162 (m), 1102 (m), 1017 (s), 960 (m, MoO), 800 (br), 555 (s) cm^{-1}. UV/vis (THF; λ_{max}, nm (ε, M^{-1} cm^{-1})]: 328 (11325), 387 (9545), 468 (3510).

RESULTS AND DISCUSSION

Ligand Synthesis. Initial attempts to prepare the monosubstituted 1*H*-pyrrole-5-isopropyl-2-carbaldehyde via an in situ Vilsmeier formylation of pyrrole followed by Friedel−Crafts alkylation[23,24] yielded a mixture of the 4- and 4,5-substituted products. Hence, the synthesis of 1*H*-pyrrole-4,5-diisopropyl-2-carbaldehyde was pursued, and optimized conditions for its synthesis were developed. Subsequent Schiff base condensation with 4-*tert*-butylaniline yielded ligand ^{iPr2}**HL** (Scheme 1).

The 2,4,5-substitution pattern of 1*H*-pyrrole-4,5-diisopropyl-2-carbaldehyde is proven by NMR spectroscopy as well as by single-crystal XRD (Figure 1). The substituted pyrrole-2-carbaldehyde forms centrosymmetric dimers with NH···O hydrogen bonds in the solid state [N···O distance 2.862(2) Å] similar to the imine chelate ligand ^{H2}**HL**.[12] The bulky chelate ligand ^{iPr2}**HL** is readily available from 1*H*-pyrrole-4,5-diisopropyl-2-carbaldehyde and 4-*tert*-butylaniline using molecular sieves. In addition to the increased steric bulk, the pyrrole in ^{iPr2}**HL** is much more electron-rich than that in ^{H2}**HL**, which is also reflected in the bathochromic shift of the pyrrole(π) →

dx.doi.org/10.1021/ic501751p | Inorg. Chem. 2014, 53, 12416−12427

Scheme 1. Synthesis of the Bulky Ligand ^{iPr2}HL and Atom Numbering for NMR Assignments

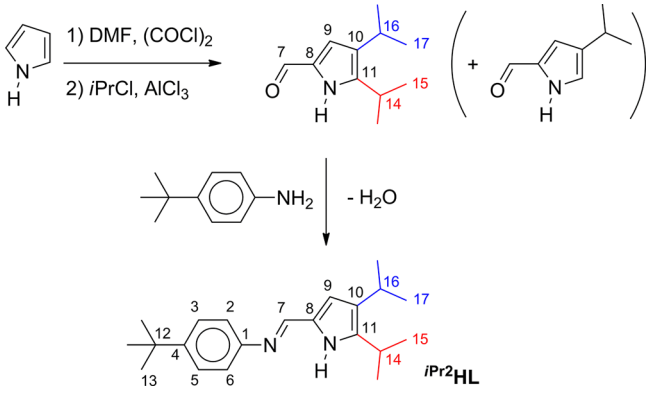

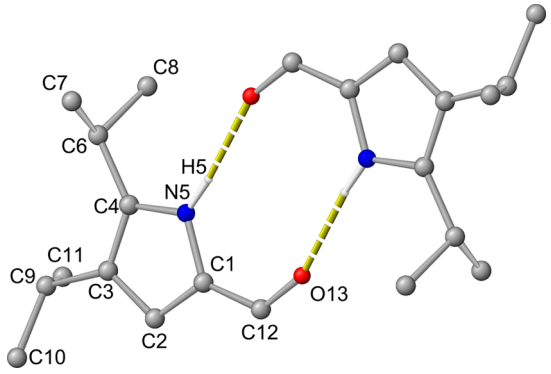

Figure 1. Molecular structure of 1*H*-pyrrole-4,5-diisopropyl-2-carbaldehyde in the crystal (CH hydrogen atoms omitted for clarity).

imine (π^*) absorption band from 329 to 343 nm.[12] Hence, the isopropyl substituents are expected to have both electronic and steric impact in metal complexes of ^{iPr2}L.

Complex Synthesis. Coordination of ^{iPr2}L to Mo^{VI} to give ^{iPr2}**1** is achieved using $MoCl_2(dme)O_2$[14] and a base (Scheme 2). In contrast to the facile deprotonation of ^{H2}HL using

Scheme 2. Synthesis of the Molybdenum Complex ^{iPr2}1 and Atom Numbering for NMR Assignments

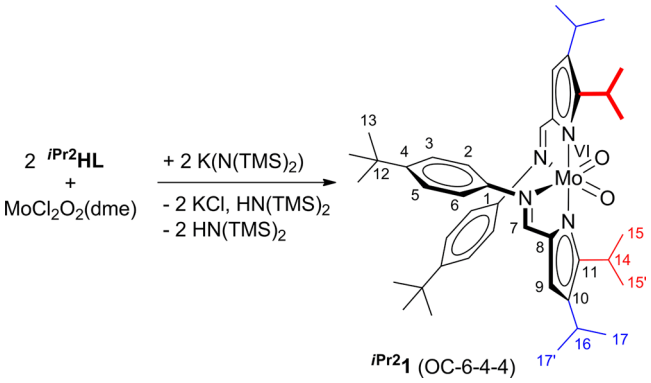

triethylamine (pK_a = 10.6), potassium bis(trimethylsilyl)amide (pK_a = 26) is required for the less acidic ^{iPr2}HL ligand. The six branched alkyl groups render the complex ^{iPr2}**1** soluble even in nonpolar solvents like hexanes. NMR (^{1}H, ^{13}C, and ^{15}N NOESY) data of ^{iPr2}**1** are fully compatible with those of ^{H2}**1**. This suggests an analogous stereochemistry of ^{H2}**1** and ^{iPr2}**1**, namely. the Δ,Λ-OC-6−4−4 configuration.[25,26] leading to a single signal set for both ligands in the NMR spectra (Scheme 2 and SI, Figure S5). However, the CH_3 groups of the isopropyl substituents in the C_2-symmetric metal complexes ^{iPr2}**1** are now diastereotopic and give distinct ^{1}H and ^{13}C NMR resonances ($H^{15,15'}$, $H^{17,17'}$, $C^{15,15'}$, and $C^{17,17'}$; Figure 2 and the

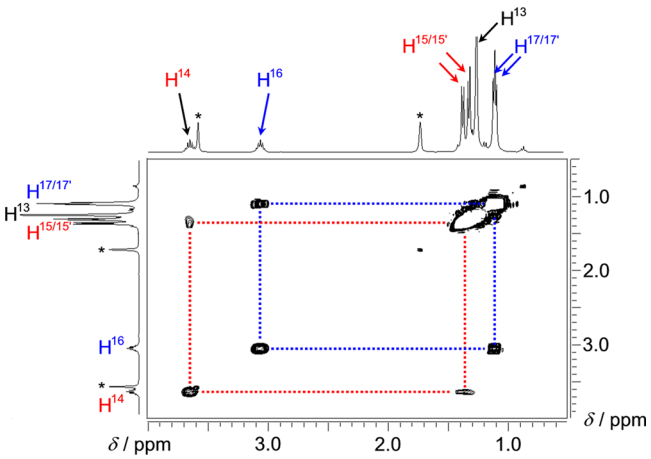

Figure 2. Partial ^{1}H^{1}H COSY of ^{iPr2}**1** in THF-d_8 showing the resonances of the diastereotopic methyl protons $H^{15/15'}$ and $H^{17/17'}$. The asterisks denote THF resonances.

Experimental Section). The CH resonance of the isopropyl group adjacent to molybdenum H^{14} is shifted to lower field by $\Delta\delta$ = 0.53 ppm compared to the free ligand, which is probably due to a sterically induced short CH···O=Mo contact in this stereoisomer. The $C^{14}H$ vector indeed points to the MoO unit with a H···O distance of 2.13 Å according to DFT (IEFPCM, THF) calculations (SI, Figure S6). This contact and the stereochemistry of ^{iPr2}**1** is further confirmed by a single-crystal XRD analysis (Figure 3). The Mo−N^P distances in ^{iPr2}**1** [2.1081(18) and 2.1016(18) Å] are slightly larger than those in ^{H2}**1** [2.0656−2.0806(22) Å]. All other metrical data are essentially identical with those of ^{H2}**1**.[12]

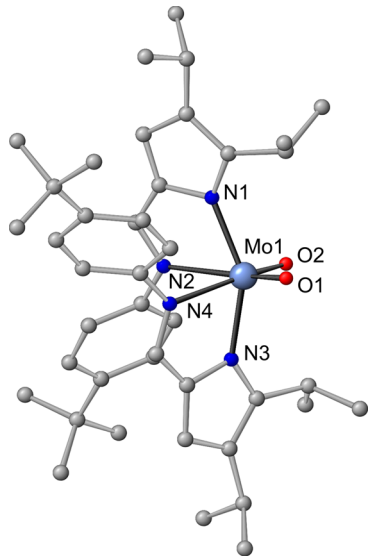

Figure 3. Molecular structure of ^{iPr2}**1** in the crystal (hydrogen atoms omitted for clarity).

dx.doi.org/10.1021/ic501751p | *Inorg. Chem.* 2014, 53, 12416−12427

As expected from the similar Mo=O distances determined by XRD, the MoO stretching modes of ^{iPr2}**1** (932/900 cm^{-1}) are very similar to those of ^{H2}**1** (928/902 cm^{-1}),[12] suggesting only a weak electronic influence of the *i*Pr groups onto the bonding of the oxido ligands coordinated cis to the pyrrolates. However, similar to the ligand pair ^{H2}**HL**/^{iPr2}**HL**, the electron-donating *i*Pr groups modify the electronic transitions involving the pyrroles in the complex pair ^{H2}**1**/^{iPr2}**1**. The pyrrole(π) → imine(π^*) charge transfer is red-shifted from 303 to 322 nm, and the pyrrole(π) → MoO_2(π^*) charge transfer is shifted from 436 to 447 nm in THF (SI, Figure S7, for relevant molecular orbitals calculated by DFT methods).[12] In full agreement with this electron-rich ligand, the reduction potential of the ^{iPr2}**1** complex (−1.78 V in THF vs Fc/Fc$^+$) is much more negative than that of ^{H2}**1** (−0.86 V in THF vs Fc/Fc$^+$)[12].

Reduction of ^{iPr2}1 to Mo^V. The chemical reduction of ^{iPr2}**1** is successful using the strong reductant decamethylcobaltocene in CH_2Cl_2 ($E_{1/2}$ = −1.94 V vs Fc/Fc$^+$ in CH_2Cl_2).[27] The presence of the decamethylcobaltocenium ion is clearly indicated by the ESI-MS spectrum. The charge-transfer absorption of ^{iPr2}**1** is shifted to 429 nm in the reduced species in CH_2Cl_2 (SI, Figure S8). The EPR spectrum of the resulting solution shows a dominant isotropic signal at g_{iso} = 1.9439 along with a satellite spectrum of $^{95/97}$Mo isotopomers (natural abundance 25%, I = $^5/_2$) with A_{iso}($^{95/97}$Mo) = 44 G (Figure 4).

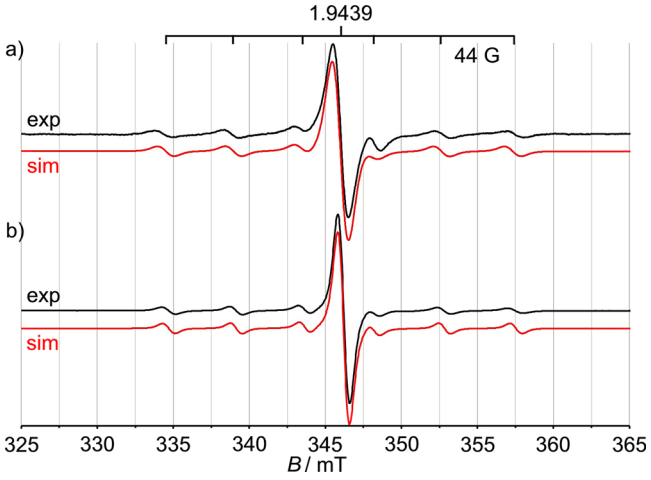

Figure 4. X-band EPR spectra of (a) ^{H2}**1**/$CoCp_2$ and (b) ^{iPr2}**1**/$CoCp^*_2$ in CH_2Cl_2 at 298 K; ν = 9.42 GHz and simulations (in red[16]).

In a frozen CH_2Cl_2 solution at 77 K, an anisotropic spectrum with $g_{1,2,3}$ = 1.9664, 1.9450, and 1.9248 is observed. Very similar spectra were obtained upon reduction of the unhindered complex ^{H2}**1** in CH_2Cl_2 [g_{iso} = 1.9459; A($^{95/97}$Mo) = 44 G]. The reported $^{95/97}$Mo coupling constant of reduced ^{H2}**1** in THF is slightly different possibly because of the different ion pairing in that solvent.[10c] Hence, no dramatic differences between reduced ^{iPr2}**1** and reduced ^{H2}**1** are discernible, suggesting similar geometries and spin densities. For scorpionatomolybdenum(V) complexes with two oxido ligands prepared by reduction of the parent dioxidomolybdenum(VI) complex with cobaltocene, g_{iso} ≈ 1.908 and A_{iso} ≈ 51 G have been reported.[8h] The MoO stretching vibrations of ^{iPr2}**1** are shifted from 932/900 to 874/801 cm^{-1} ($\Delta\tilde{\nu}$ = 58/99 cm^{-1}) in a fashion similar to that observed for dioxidomolybdenum(VI/V) complexes with scorpionato ligands (937/904 to 896/792 cm^{-1}; $\Delta\tilde{\nu}$ = 41/112 cm^{-1}; Chart 1, **B**).[8h] Hence, we assign the observed EPR resonances to a [Mo^{V}O$_2$]$^+$ species.

OAT. The previously reported dioxidomolybdenum(VI) complexes (Chart 1, **E** and **G**) are competent to transfer an oxygen atom to phosphanes to give phosphane oxides. In all cases, the resulting free coordination site at Mo^{IV} is filled either by a residual [Mo^{VI}O$_2$]$^{2+}$ complex to give a stable purple binuclear μ-oxido [Mo$^V_2$O$_3$]$^{4+}$ complex ^{R2}**3** or by excess PMe_3 to give green isolable phosphane complex ^{R2}**2** after longer reaction times (Scheme 3). The intermediate μ-oxido complex ^{R2}**3** only reacts slowly with PMe_3.[10] On the basis of DFT calculations and NMR studies, the local OC-6−4−4 configuration was also assigned to the Mo^V centers in diamagnetic bimetallic ^{R2}**3**. This is now fully corroborated by XRD analysis of ^{H2}**3** (Figure 5). As expected, the complex is centrosymmetric with a linear Mo−O−Mo moiety, transoid-oriented Mo=O units, and local OC-6−4−4 configurations of the Mo^V sites. Because of the different types of oxido ligands, the chelate ligands of one molybdenum site become chemically different and give two characteristic signal sets in the NMR spectra.[10a,b] The Mo=O and Mo−μ-O bond lengths amount to 1.6720(13) and 1.8742(15) A, respectively.

Treatment of the bulkier complex ^{iPr2}**1** with PMe_3 directly leads to yellow-green phosphane complex ^{iPr2}**2** (Scheme 3) without noticeable intermediate formation of bimetallic complex ^{iPr2}**3**. In fact, all attempts to detect intermediate

Scheme 3. OAT Reactions of ^{H2}1 and ^{iPr2}1 to PMe_3 and Atom Numbering for NMR Assignments

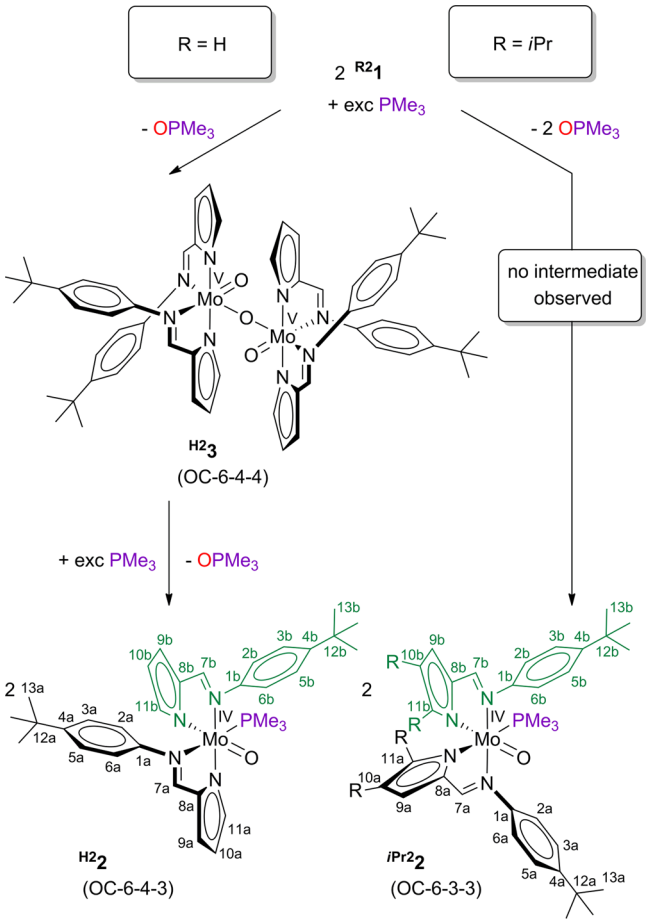

dx.doi.org/10.1021/ic501751p | Inorg. Chem. 2014, 53, 12416−12427

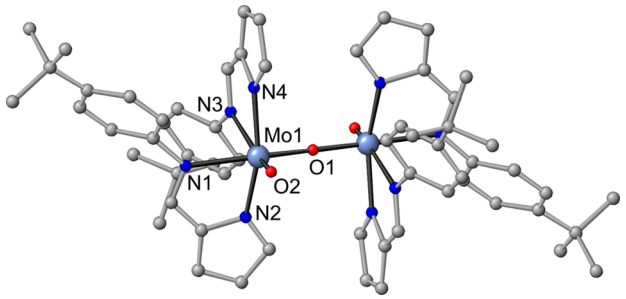

Figure 5. Molecular structure of ^{H2}**3** in the crystal (hydrogen atoms omitted for clarity).

binuclear μ-oxidomolybdenum(V) complex ^{iPr2}**3** by NMR or UV/vis spectroscopy were unsuccessful during the reaction with PMe_3.

Monitoring the reaction of ^{iPr2}**1** with the small-cone-angle[28] ligand PMe_3 by ^{31}P NMR spectroscopy reveals the formation of three stereoisomeric phosphane complexes in a 25:5:1 ratio with ^{31}P NMR resonances at δ −1.70, −1.95, and −1.49, respectively. For the major isomer ^{iPr2}**2**, we were able to assign all ^{1}H and ^{13}C NMR resonances of the two chemically different chelate ligands a and b (Scheme 3) by ^{1}H^{15}N HMBC, ^{1}H^{1}H COSY, ^{1}H^{1}H NOESY, ^{1}H^{13}C HSQC, ^{1}H^{13}C HMBC, and ^{1}H^{31}P HMBC spectra. The ^{15}N resonances of ^{iPr2}**2** are significantly different from those of the less hindered complex ^{H2}**2** concerning both absolute chemical shift values and the signal pattern. This already suggests a fundamental stereochemical difference between ^{H2}**2** and ^{iPr2}**2**.[12] Several nuclear Overhauser effect (NOE) cross peaks between PMe_3 protons and *both* aryl ring protons $H^{2a,6a}$ and $H^{2b,6b}$ are observed, suggesting close contact of PMe_3 to both aryl rings (Figure 6a). This is only possible with the imine nitrogen atoms N^{ia} and N^{ib} located in the cis position to the phosphane (OC-6−3−3 or OC-6−3−4 configuration; Figure 7).[25,26] Interchelate NOE cross peaks for $H^{14a} \leftrightarrow H^{7b}$ and $H^{14a} \leftrightarrow H^{2b,6b}$ and vice versa for $H^{14b} \leftrightarrow H^{7a}$ and $H^{14b} \leftrightarrow H^{2a,6a}$ place N^{pa} cis to N^{ib} and vice versa N^{pb} cis to N^{ia} (Figure 6b). This is only accomplished in the OC-6−3−3 and OC-6−4−4 isomers. Taken together, only the OC-6−3−3 configuration accounts for the observed contacts in ^{iPr2}**2**. A cross peak from PMe_3 to H^{14b} places N^{pb} cis to PMe_3, and a cross peak from PMe_3 to $H^{3a,5a}$ places the aryl ring of ligand a in closer contact with PMe_3 (Figure 6a), which allows one to unambiguously assign the position of the different chelates a and b relative to PMe_3.

In OC-6−4−3 isomers (^{H2}**2**), a characteristic splitting of H^{7a} by coupling to ^{31}P of $^4J_{PH}$ = 2.3 Hz is typically observed (Scheme 2).[10,12] No such large couplings are found in ^{iPr2}**2** either for H^{7a} or for H^{7b}, also arguing against N^{ia} trans to PMe_3, i.e., placing both N^{ia} and N^{ib} cis to PMe_3. From the models (Figure 7), it becomes immediately clear that steric interactions between the PMe_3 ligand and the isopropyl group (H^{14a}) are present in the OC-6−4−3 and OC-6−4−4 isomers of ^{iPr2}**2**, which are, hence, destabilized. In summary, the bulkier ligand changes the stereochemical course of the OAT to give OC-6−3−3 as the major isomer instead of the preferred OC-6−4−3 isomer of ^{H2}**2**.

The different stereochemistry manifests itself also in different Mo=O stretching frequencies, with that of ^{iPr2}**2** (946 cm^{-1}) being larger than that of ^{H2}**2** (935 cm^{-1}).[12] Furthermore, the ligand-field bands of the d^2 complex ^{iPr2}**2** (685 and 505 nm) are also distinguished from those of ^{H2}**2** (715, 610, and 479 nm)

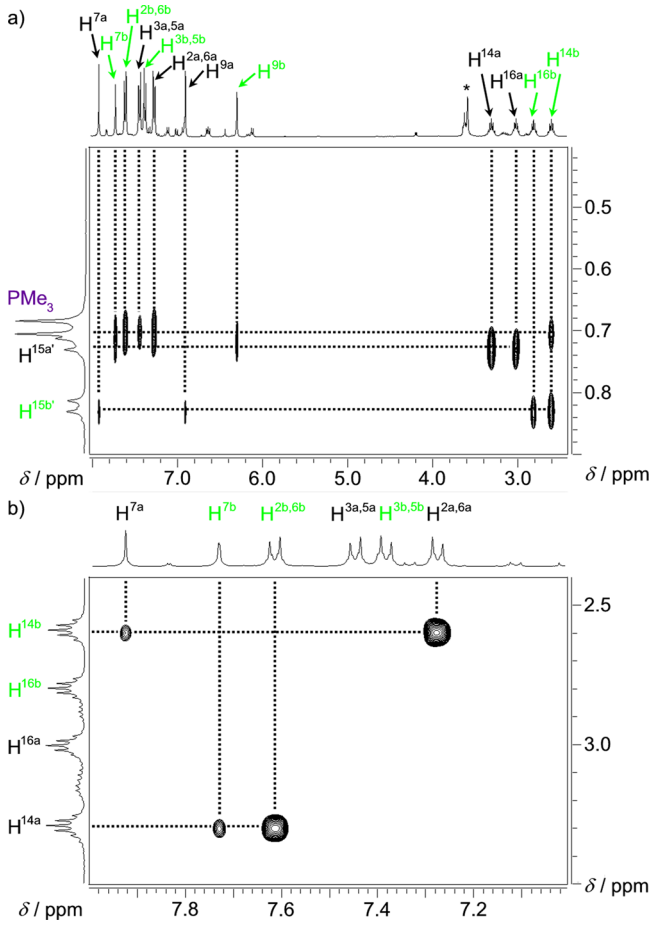

Figure 6. Partial ^{1}H^{1}H NOESY of ^{iPr2}**2** in THF-d_8 showing (a) contacts of PMe_3 to the chelates a and b and (b) contacts between chelates a and b. The asterisks denote THF resonances.

because of the different complex geometries and ligand-field strengths.[12]

In order to hamper phosphane coordination at the free coordination site generated by OAT, we employed the much bulkier PPh_3 (Tolman cone angle 145°)[28] instead of PMe_3 (Tolman cone angle 118°).[28] Treating ^{iPr2}**1** with excess PPh_3 in THF (Scheme 4) also results in OAT, liberating $OPPh_3$ [δ(^{31}P) 23.9].

After standing for several weeks, a few yellow plates crystallized from the THF solution. These were identified as the di(μ-oxido)molybdenum(V) complex ^{iPr2}**4**·THF by XRD (Figure 8). The dinuclear complex ^{iPr2}**4**·THF features a *syn*-$[Mo_2O_4]^{2+}$ core and only one chelate ligand per Mo^V atom. Hence, dissociation of one chelate ligand and oxidation of the metal centers must have occurred during the long crystallization time.

The Mo···Mo distances of ^{iPr2}**4**·THF amount to 2.5593(15)/2.5629(13) Å, similar to that of $[(NacNac)MoO]_2(\mu\text{-}O)_2$ [2.5591(5) Å;[30] NacNacH = $CH[C(Me)N(2,6\text{-}Me_2C_6H_3)]_2$] but somewhat shorter than those of comparable complexes with pentacoordinate molybdenum(V) complexes (2.587−2.623 Å[31−34]). A bridging THF molecule is loosely associated with the molybdenum centers with Mo1···O100 and Mo2···O101 (second independent molecule) distances of 2.8331(50) and 2.7731(52) Å, respectively (Figure 8). When this THF molecule and the Mo···Mo interaction are neglected, the Mo^V centers in ^{iPr2}**4**·THF are closer to a C_{4v}-symmetric than to a

dx.doi.org/10.1021/ic501751p | *Inorg. Chem.* 2014, 53, 12416−12427

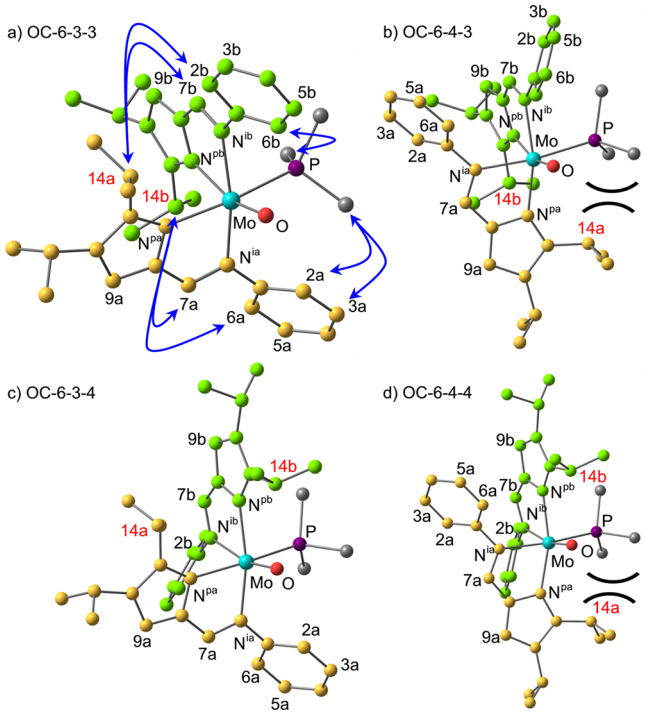

Figure 7. DFT-calculated minimum geometries of possible stereoisomers of ^{iPr2}**2** (the chelate ligands a and b are color-coded yellow and green; NOE contacts are indicated by blue allows; hydrogen atoms omitted for clarity).

Scheme 4. OAT of ^{iPr2}1 to PPh_3 and Follow-up Reactions

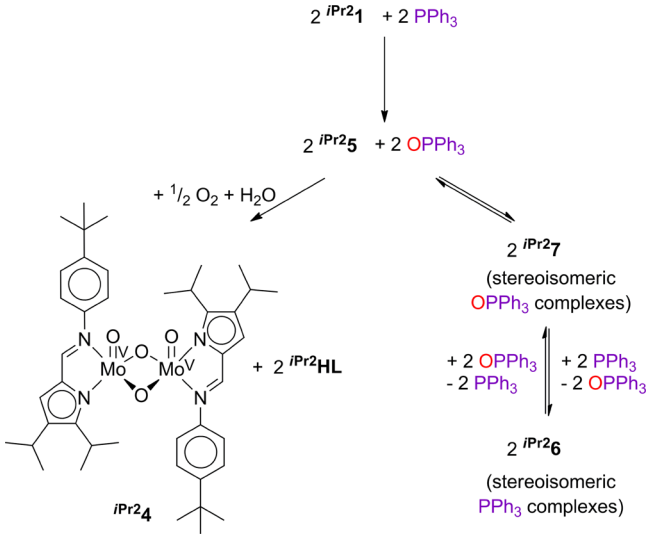

D_{3h}-symmetric arrangement, with the terminal oxido ligand in the axial position (indexes of trigonality τ = 0.06/0.13[29]). The reported $[(NacNac)MoO]_2(\mu\text{-}O)_2$ complex is between a square pyramid and a trigonal bipyramid (τ = 0.52).[30] DFT (IEFPCM, THF) calculations correctly reproduce the local square-pyramidal structure of ^{iPr2}**4**·THF with τ = 0.04/0.09 (SI, Figure S9). In a CsI disk, the symmetric and antisymmetric Mo═O and Mo−O−Mo vibrations of ^{iPr2}**4**·THF are found at 970/959 and 698/692 cm^{-1}, respectively. This agrees reasonably well with the scaled DFT (IEFPCM, THF)-calculated harmonic vibrations of ^{iPr2}**4**·THF at 948/925 and 707/686 cm^{-1} (scaled by 0.9614[35]). The Mo═O stretch is

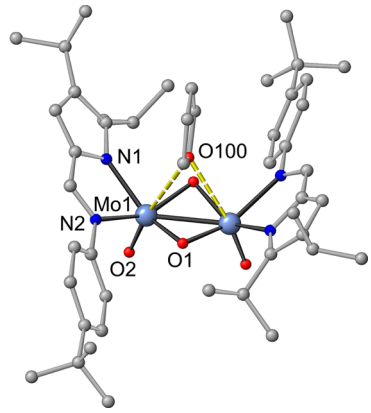

Figure 8. Molecular structure of ^{iPr2}**4**·THF in the crystal (hydrogen atoms omitted for clarity; only one dinuclear complex of the two independent molecules is shown).

higher in energy than those of comparable *syn*-$[Mo_2O_4]^{2+}$ complexes with pentacoordinate Mo^V (927−959 cm^{-1}).[30,33,34,36,37] The stable dinuclear structure of ^{iPr2}**4**·THF is further proven by its FD-MS spectrum, showing a molecular-ion peak at m/z 875 for ^{iPr2}**4** with correct isotopic distribution for two molybdenum centers (SI, Figure S10). The NMR spectra (^{1}H, ^{13}C, and ^{15}N) of ^{iPr2}**4** each feature a single set of resonances consistent with the C_2-symmetric dinuclear structure (SI, Figure S5). Diastereotopic methyl protons of the isopropyl groups $H^{15,15'}$ and $H^{17,17'}$ corroborate coordination of the ligand. Furthermore, the sharpness of the NMR resonances of ^{iPr2}**4** proves its diamagnetic nature.

Monitoring the reaction of ^{iPr2}**1** with 5 equiv of PPh_3 in benzene by ^{1}H and ^{31}P NMR as well as by UV/vis spectroscopy reveals that ^{iPr2}**4** is not produced at all at short time scales under rigorous exclusion of water (SI, Figure S11). Indeed, the ^{1}H NMR resonances of ^{iPr2}**1** are replaced by a different signal pattern with many overlapping resonances. The decay of ^{iPr2}**1** (monitored at δ 4.0, H^{14} in C_6D_6) parallels the formation of $OPPh_3$ (δ 7.75, H^{ortho} in C_6D_6), suggesting a successful OAT reaction. The ^{31}P NMR resonances at δ 25.9 and −3.6 ($OPPh_3$ and PPh_3, respectively) in C_6D_6 are broad at room temperature but sharpen upon increasing temperature to 343 K (likely because of increasing solubilities; SI, Figure S12). In toluene-d_8, the ^{31}P NMR resonances are sharp already at 295 K (SI, Figure S13). Distinct resonances for coordinated PPh_3 or $OPPh_3$ are not observed, neither at room temperature (C_6D_6) nor at 243 K (toluene-d_8). However, the ^{31}P NMR resonance of PPh_3 is shifted from that of pure PPh_3 (δ −4.8 in C_6D_6; SI, Figure S14) by 1.2 ppm. The observed integrated $OPPh_3$:PPh_3 ratio corresponds to 0.27 for the reaction of ^{iPr2}**1** with 5 equiv of PPh_3 at 295 K (SI, Figure S14). The integral ratio (0.24) becomes more accurate at higher temperature because of the better solubility (343 K, SI, Figure S12). The predicted ratio for the simple OAT reaction (eq 1) is 0.25.

$$^{iPr2}\mathbf{1} + 5PPh_3 \rightarrow {}^{iPr2}\mathbf{5} + OPPh_3 + 4PPh_3 \quad (1)$$

For OAT and subsequent comproprtionation with residual ^{iPr2}**1** (eq 2), a ratio of 0.11 is calculated.

$$2\,{}^{iPr2}\mathbf{1} + 10PPh_3 \rightarrow {}^{iPr2}\mathbf{3} + OPPh_3 + 9PPh_3 \quad (2)$$

Hence, the ^{31}P NMR data fit to reaction (1). To deduce the identity and fate of the initially formed pentacoordinate ^{iPr2}**5**,

dx.doi.org/10.1021/ic501751p | Inorg. Chem. 2014, 53, 12416−12427

we performed several experiments (^{1}H NMR, MS, DFT calculations, UV/vis/NIR spectroscopy, and DOSY).

The ^{1}H NMR spectrum of ^{iPr2}**1** and 2 equiv of PPh_3 in C_6D_6 after several hours shows resonances for two ligand sets a/b in a ratio of 1:1, with all resonances assigned to the respective nuclei by homonuclear COSY and NOESY experiments. ^{13}C NMR resonances are assigned on the basis of $^1H^{13}C$ HSQC and HMBC experiments (SI, Figures S15–S18). The presence of two stereochemically distinct ligands a and b suggests a chelate/Mo ratio of 2:1 in a C_1-symmetric complex. The FD-MS spectrum of the reaction mixture shows peaks at m/z 278 (100%, $OPPh_3$), 745 (^{iPr2}**1**, 1%), 766 (unknown, 4%), and 875 (^{iPr2}**4**, 2%). No hints for dinuclear $[Mo_2O_3]^{4+}$ complexes were found, although this is typically observed with ^{H2}**3**. Indeed, molecular models show that a dinuclear centrosymmetric $[Mo_2O_3]^{4+}$ complex with a configuration of ^{H2}**3** (OC-6–4–4) is sterically impossible because of the isopropyl groups as expected. OC-6–4–3 and OC-6–3–4 $[Mo_2O_3]^{4+}$ complexes are impossible as well. A dinuclear $[Mo_2O_3]^{4+}$ complex ^{iPr2}**3** is only feasible with OC-6–3–3 configurations of the local MoO_2 units, as suggested by DFT calculations albeit with severe steric constraints concerning the aryl rings and significantly elongated Mo–O bonds from 1.884 Å[10b] to 1.905/1.907 Å (SI, Figure S19). Consistent with steric hindrance, the dimer ^{iPr2}**3** is calculated to be highly unstable with respect to disproportionation into $[Mo^{VI}O_2]^{2+}$ ^{iPr2}**1** and $[Mo^{IV}O]^{2+}$ ^{iPr2}**5** by 86 kJ mol^{-1} (DFT, IEFPCM, THF). The purple dinuclear complex ^{H2}**3** (OC-6–4–4) shows characteristic π–π^* bands of the Mo–O–Mo core around 550 nm (SI, Figure S20).[10a,b] For ^{iPr2}**3** (OC-6–3–3), time-dependent DFT calculations on ^{iPr2}**3** (OC-6–3–3) predict intense charge-transfer bands at 999, 798, and 593 nm. No such absorption bands are found in the reaction mixture of ^{iPr2}**1** and PPh_3 up to 2200 nm (Figure 9 and SI, Figure S21). Instead, absorption bands at 329 and 456 nm are observed, similar to the charge-transfer bands of the PMe_3 complex ^{iPr2}**2** (345 and 425 nm; see the Experimental Section). All of the combined experimental and modeling data suggest that dinuclear complex ^{iPr2}**3** is not formed at all.

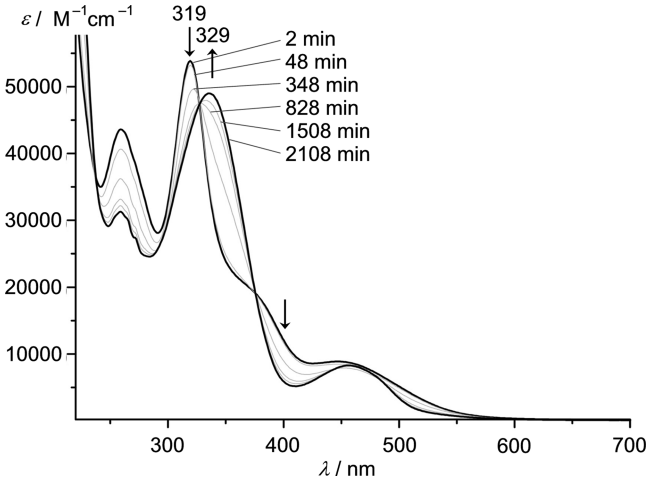

Figure 9. Evolution of the UV/vis spectra of ^{iPr2}**1** in petroleum ether 40–60 °C with 2 equiv of PPh_3.

Diffusion coefficients of the final product, as well as of ^{iPr2}**1**, ^{iPr2}**2**, ^{H2}**3**, and ^{iPr2}**4**, were determined by DOSY in C_6D_6 at 298 K (SI, Figures S22–S26). A diffusion coefficient of log D/m^2 s^{-1} = −9.3 is found at room temperature for the final product. This indicates slower diffusion of the product than the starting complex ^{iPr2}**1** with log D/m^2 s^{-1} = −9.2 and, hence, a larger molecular size. This is inconsistent with genuine pentacoordinate $[Mo^{IV}O]^{2+}$ complex ^{iPr2}**5**. For the unsubstituted complex ^{H2}**1** and its corresponding dinuclear $[Mo^{V}_2O_3]^{4+}$ complex ^{H2}**3**, strongly different diffusion coefficients of log D/m^2 s^{-1} = −9.0 and −9.3 are measured, respectively. Hence, the final product of the reaction ^{iPr2}**1** and PPh_3 is neither dinuclear complex ^{iPr2}**3** nor pentacoordinate complex ^{iPr2}**5**, but a complex of intermediate size. Hence, we suggest labile coordination of PPh_3 or OPh_3 to give PPh_3 or $OPPh_3$ complexes ^{iPr2}**6** or ^{iPr2}**7**, similar to the PMe_3 complex ^{iPr2}**2** although with unknown stereochemistry (SI, Figures S27 and S28, for DFT-calculated structures of ^{iPr2}**6** and ^{iPr2}**7**). The DFT-calculated Mo–P bond lengths of the stereoisomers of ^{iPr2}**2** increase from 2.594, 2.587, 2.583, and 2.580 Å to 2.770, 2.756, 2.712, and 2.658 Å in the corresponding stereoisomers of ^{iPr2}**6** (Figure 7 and SI, Figure S27). This finding is consistent with a rather weak PPh_3 coordination. ^{31}P–^{1}H correlations are observed in the $^1H^{31}P$ HMBC spectrum assignable to coordinated PPh_3 and $OPPh_3$ at δ −10 and 18, respectively, consistent with this interpretation (SI, Figure S29).

Temporal evolution of the reaction has been monitored by UV/vis and ^{1}H NMR spectroscopy. The UV/vis spectra of ^{iPr2}**1** and 2 equiv of PPh_3 in petroleum ether 40–60 °C show a gradual decrease of the 319 nm absorption band of ^{iPr2}**1** and a rise of the 329 nm band (Figure 9). The 446 nm band of ^{iPr2}**1** decreases in the first 60 min and is then replaced by a band at 456 nm. No clean isosbestic points are observed over 35 h, suggesting a consecutive reaction. A similar picture is observed in the ^{1}H NMR spectra in C_6D_6 (SI, Figure S11). Indeed, one set of ^{1}H NMR resonances (two ligand sets a and b) rapidly appears [monitored, e.g., at δ 4.77 (pseudo sept) and 0.77 (d), "rapid signals"] and subsequently slightly decays, reaching a steady-state concentration. A second set of resonances [monitored at at δ 3.45 (pseudo sept) and 1.71 (d), "slow signals"] evolves subsequently (SI, Figure S30). The final ratio of the "rapid species" to the "slow species" is approximately 1:4. These observations are consistent with the rapid deoxygenation of ^{iPr2}**1** to a kinetic product ("rapid species") and its equilibration with the thermodynamically favored product ^{iPr2}**6**/^{iPr2}**7** ("slow species"). DOSY experiments at early and late stages of the reaction reveal similar self-diffusion coefficients for the rapid and slow species (both log D/m^2 s^{-1} = −9.3), suggesting similar molecular volumes. Hence, the rapid and slow species are assigned to PPh_3/$OPPh_3$ complexes with different stereochemistries. A similar equilibration between stereoisomers via a dissocative trigonal twist was recently elucidated with coordinated *tert*-butylisonitrile instead of phosphanes.[10d] Unfortunately, severe overlap with PPh_3/$OPPh_3$ resonances and resonances of a further minor species (possibly a further PPh_3/$OPPh_3$ stereoisomer; SI, Figures S27 and S28) prevents detailed stereochemical analyses by NOE spectroscopy in this case.

At this point, we conclude that ^{iPr2}**HL** is sufficiently sterically encumbered to prevent dinucleation, in contrast to many other reported sterically demanding ligands, but still allows for labile PPh_3/$OPPh_3$ coordination (^{iPr2}**6**/^{iPr2}**7**). Future experiments aim at even bulkier ligands ^{R2}**HL** (with, e.g., R = *t*Bu) and bulkier phosphanes PR_3[28] to provide a truly pentacoordinate $[Mo^{IV}O]^{2+}$ complex for further chemical transformations. The affinity of PR_3 to molybdenum should be diminished in higher oxidation states of molybdenum. Hence, oxidation of the well-

dx.doi.org/10.1021/ic501751p | *Inorg. Chem.* 2014, 53, 12416–12427

characterized hexacoordinate complex ^{iPr2}**2** was probed by electrochemical and chemical means.

Oxidation of ^{iPr2}2 to Mo^{V}. The sterically unencumbered yet stable complex ^{H2}**2** is irreversibly oxidized at E_p = −0.29 V versus ferrocene. Presumably, dinucleation prevents a reversible redox process.[12] With the *tert*-butylimido analogue of ^{H2}**2**, reversible oxidation ($E_{1/2}$ = −0.71 V; Chart 1, **F**) to the respective Mo^{V} complex had been achieved because of steric protection by the *tert*-butylimido ligand.[12] The cyclic voltammogram of the novel sterically shielded Mo^{IV} complex ^{iPr2}**2** in THF/(nBu$_4$N)[B(C$_6$F$_5$)$_4$] reveals a quasi-reversible oxidation wave at $E_{1/2}$ = −0.40 V (SI, Figure S31). In essence, steric protection of the [Mo^{V}O]$^{3+}$ unit by two aryl groups sufficiently stabilizes the mononuclear [Mo^{V}O(PMe$_3$)]$^{+}$ complex [^{iPr2}**2**]$^{+}$ on the time scale of the CV experiments, and [^{iPr2}**2**]$^{+}$ should be experimentally detectable on short time scales.

Chemical oxidation of the phosphane complex ^{iPr2}**2** to [^{iPr2}**2**]$^{+}$ with AgSbF$_6$ in THF ($E_{1/2}$ = 0.41 V vs Fc/Fc^{+})[27] gives an initial doublet EPR signal at g = 1.9667, A($^{95/97}$Mo) = 33.5 G, and A(^{31}P) = 18.0 G. This doublet is replaced by a singlet resonance at g = 1.9455 and A($^{95/97}$Mo) = 47.0 G within 30 min at 295 K (Figure 10). Evolution of the EPR spectra occurs,

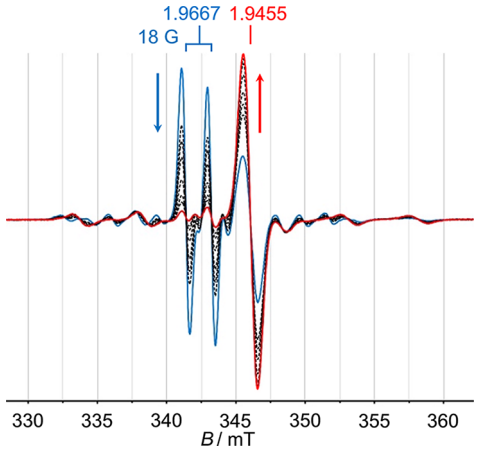

Figure 10. Evolution of the X-band EPR spectra of ^{iPr2}**2**/AgSbF$_6$ in THF at 295 K within 30 min; ν = 9.42 GHz.

with several isosbestic points suggesting a clean conversion between two EPR-active species. This observation is straightforwardly explained by the formation of an intermediate PMe$_3$ complex (strong superhyperfine coupling to ^{31}P; small hyperfine coupling to $^{95/97}$Mo), which is subsequently replaced by a molybdenyl [Mo^{V}O]$^{3+}$ complex lacking the phosphane ligand. The increased coupling constant to $^{95/97}$Mo also supports the loss of the PMe$_3$ ligand, which was able to delocalize the spin density in [^{iPr2}**2**]$^{+}$. The molybdenum(V) phosphane complex of the imido analogue of ^{H2}**2** was even stable for extended periods of time [g = 1.9810, A($^{95/97}$Mo) = 40.3 G, and A(^{31}P) = 28.7 G; OC-6−4−3 isomer].[12] For the polymer-immobilized analogue of ^{H2}**2**, a superhyperfine coupling constant to the phosphorus nucleus of A(^{31}P) ≈ 24 G had been estimated from anisotropic EPR spectra.[10a] DFT calculations estimate a superhyperfine coupling constant to phosphorus of 10.5 G (OC-6−3−3 isomer [^{iPr2}**2**]$^{+}$), in acceptable agreement with the experimental value. [^{iPr2}**2**]$^{+}$ slowly releases the PMe$_3$ ligand to give a single product that might be a positively charged pentacoordinate [Mo^{V}O]$^{3+}$ or a hexacoordinate [Mo^{V}O(THF)]$^{3+}$ complex. In accordance with this view, the MoO stretching vibration (as CsI disk) shifts from 946 cm^{-1} (^{iPr2}**2**) to 960 cm^{-1} in the final Mo^{V} product. Furthermore, the $^{95/97}$Mo coupling constant is increased from 33.5 to 47.0 G, reflecting the stronger confinement of the unpaired electron on the molybdenum center in the PMe$_3$ free complex. Coordination of the SO_3^{2-} substrate to Mo^{V} has also been suggested for a mutant of human sulfite oxidase by EPR spectroscopy by Enemark and co-workers.[38] It is conceivable that coordination of a two-electron donor ligand (PMe$_3$ and SO_3^{2-}) to Mo^{IV} lowers its oxidation potential and hence contributes to the overall efficiency of the catalytic cycle. Subsequently, the bound donor ligand is released from Mo^{V} and replaced by water/hydroxide. The feasibilty of the release of the donor ligand due to oxidation of the metal center is exemplified by the oxidation of ^{iPr2}**2** and documented by evolution of the EPR spectra (Figure 10).

CONCLUSION

A novel bulky Schiff base chelate ligand ^{iPr2}**HL** bearing two isopropyl groups and its Mo^{VI}(^{iPr2}**L**)$_2$O$_2$ complex ^{iPr2}**1** have been prepared. In spite of the increased steric shielding, ^{iPr2}**1** is active in OAT to PMe$_3$ and to PPh$_3$ to give OPMe$_3$ and OPPh$_3$, respectively. PMe$_3$ fills the vacant coordination site to give a stable hexacoordinate Mo^{IV}(^{iPr2}**L**)$_2$O(PMe$_3$) complex ^{iPr2}**2** with OC-6−3−3 stereochemistry, while PPh$_3$/OPPh$_3$ seems to be only weakly associated with the Mo^{IV} center in ^{iPr2}**6**/^{iPr2}**7** (stereochemistry unknown). Dinuclear complexes of the type [Mo^{V}(^{iPr2}**L**)$_2$O]$_2$(μ-O) ^{iPr2}**3** were not observed. On the other hand, the labile complexes ^{iPr2}**6**/^{iPr2}**7** are highly susceptible to chelate dissociation/metal oxidation, giving a dinuclear di(μ-oxido) [Mo^{V}(^{iPr2}**L**)O]$_2$(μ-O)$_2$ complex ^{iPr2}**4**·THF with reduced steric congestion.

Upon one-electron oxidation of the PMe$_3$ complex ^{iPr2}**2** to Mo^{V} with Ag^{+}, coordinated PMe$_3$ is slowly liberated, leaving a free coordination site at the [Mo^{V}O]$^{3+}$ unit. The results underscore the possibility that substrate coordination (PR$_3$ and SO_3^{2-}) at Mo^{IV} and Mo^{V} during turnover might also be relevant for enzymes of the molybdenum-containing oxidase family.

Furthermore, the reported findings pave the way for future chemistry at the "free coordination site" of monooxido [Mo^{IV}O]$^{2+}$ and [Mo^{V}O]$^{3+}$ complexes using the novel bulky ligand ^{iPr2}**HL**. The current work encompasses reactions of [Mo^{IV}O]$^{2+}$ and [Mo^{V}O]$^{3+}$ complexes with small monodenate ligands that are relevant for functional biomimetic models of molybdenum-containing enyzmes and with main-group elements that are relevant for atom-transfer reactions.

ASSOCIATED CONTENT

Supporting Information

Crystallographic data in CIF format, molecular structures of 1*H*-pyrrole-4,5-diisopropyl-2-carbaldehyde, ^{iPr2}**1**, ^{H2}**3**, and ^{iPr2}**4** in the crystal, ^{1}H NMR spectra of ^{iPr2}**1** and ^{iPr2}**4**, DFT-calculated minimum geometries of ^{iPr2}**1** and ^{iPr2}**4**·THF, the only possible stereoisomer of ^{iPr2}**3**, and possible stereoisomers of ^{iPr2}**6** and ^{iPr2}**7**, frontier molecular orbitals of ^{iPr2}**1**, UV/vis spectrum of ^{iPr2}**1**, FD-MS spectrum of ^{iPr2}**4**, evolution of the ^{1}H NMR spectra of ^{iPr2}**1**, ^{31}P{^{1}H} NMR spectra of ^{iPr2}**1**, evolution of the ^{31}P{^{1}H} NMR spectra of ^{iPr2}**1**, ^{1}H^{1}H COSY and NOESY spectra of ^{iPr2}**1**, ^{1}H^{13}C HSQC and HMBC spectra of ^{iPr2}**1**, comparison of the UV/vis spectra of ^{iPr2}**1** and ^{H2}**3**, evolution of

dx.doi.org/10.1021/ic501751p | Inorg. Chem. 2014, 53, 12416−12427

the UV/vis spectra of ^{iPr2}**1**, 2D DOSY spectra of ^{iPr2}**1**, ^{H2}**1** ^{iPr2}**2**, ^{H2}**3**, and ^{iPr2}**4**, integrals of selected ^{1}H NMR resonances of ^{iPr2}**1**, cyclic voltammogram of ^{iPr2}**2**, UV/vis spectrum of ^{iPr2}**2**, and Cartesian coordinates of all optimized structures. This material is available free of charge via the Internet at http://pubs.acs.org.

AUTHOR INFORMATION

Corresponding Author

*E-mail: katja.heinze@uni-mainz.de. Fax: +49-6131-39-27277.

Author Contributions

The manuscript was written through contributions of all authors. All authors have given approval to the final version of the manuscript.

Notes

The authors declare no competing financial interest.

ACKNOWLEDGMENTS

We are grateful to Dr. Mihail Mondeshki for NMR support, to Regine Jung-Pothmann for X-ray data collection, and graduate students Stefan Pusch, Christian Muhl, and Christina M. Mrosek for preparative assistance.

REFERENCES

(1) Holm, R. H. *Chem. Rev.* **1987**, *87*, 1401.

(2) (a) Dobbek, H.; Gremer, L.; Meyer, O.; Huber, R. In *Handbook of Metalloproteins*; Messerschmidt, A., Huber, R., Wieghardt, K., Poulos, T., Eds.; Wiley: Chichester, U.K., 2001. (b) Hille, R. *Chem. Rev.* **1996**, *96*, 2757.

(3) (a) Kisker, C.; Schindelin, H.; Rees, D. C. *Annu. Rev. Biochem.* **1997**, *66*, 233. (b) Hille, R.; Nishino, T.; Bittner, F. *Coord. Chem. Rev.* **2011**, *255*, 1179. (c) Feng, C.; Tollin, G.; Enemark, J. H. *Biochim. Biophys. Acta* **2007**, *1774*, 527. (d) Johnson-Winters, K.; Tollin, G.; Enemark, J. H. *Biochemistry* **2010**, *49*, 7242.

(4) (a) Berg, J. M.; Holm, R. H. *J. Am. Chem. Soc.* **1985**, *107*, 917. (b) Gheller, S. F.; Schultz, B. E.; Scott, M. J.; Holm, R. H. *J. Am. Chem. Soc.* **1992**, *114*, 6934. (c) Schultz, B. E.; Holm, R. *Inorg. Chem.* **1993**, *32*, 4244.

(5) (a) Holm, R. H. *Coord. Chem. Rev.* **1990**, *100*, 183. (b) Enemark, J. H.; Cooney, J. J. A.; Wang, J.-J.; Holm, R. H. *Chem. Rev.* **2004**, *104*, 1175. (c) Sugimoto, H.; Tsukube, H. *Chem. Soc. Rev.* **2008**, *37*, 2609. (d) Schulzke, C. *Eur. J. Inorg. Chem.* **2011**, 1189.

(6) Doonan, C. J.; Slizys, D. A.; Young, C. G. *J. Am. Chem. Soc.* **1999**, *121*, 6430.

(7) Trofimenko, S. *J. Am. Chem. Soc.* **1966**, *88*, 1842.

(8) (a) Roberts, S. A.; Young, C. G.; Cleland, W. E., Jr.; Ortega, R. B.; Enemark, J. H. *Inorg. Chem.* **1988**, *27*, 3044. (b) Xiao, Z.; Bruck, M. A.; Enemark, J. H.; Young, C. G.; Wedd, A. G. *Inorg. Chem.* **1996**, *35*, 7508. (c) Nemykin, V. N.; Laskin, J.; Basu, P. *J. Am. Chem. Soc.* **2004**, *126*, 8604. (d) Doonan, C. J.; Millar, A. J.; Nielsen, D. J.; Young, C. G. *Inorg. Chem.* **2005**, *44*, 4506. (e) Nemykin, J.; Basu, P. *Inorg. Chem.* **2005**, *44*, 7494. (f) Sengar, R. S.; Basu, P. *Inorg. Chim. Acta* **2007**, *360*, 2092. (g) Rajapakshe, A.; Snyder, R. A.; Astashkin, A. V.; Bernardson, P.; Evans, D. J.; Young, C. G.; Evans, D. H.; Enemark, J. H. *Inorg. Chim. Acta* **2009**, *362*, 4603. (h) Ng, V. W. L.; Taylor, M. K.; White, J. M.; Young, C. G. *Inorg. Chem.* **2010**, *49*, 9460. (i) Ng, V. W. L.; Taylor, M. K.; Hill, L. M. R.; White, J. M.; Young, C. G. *Eur. J. Inorg. Chem.* **2010**, 3261. (j) Ng, V. W. L.; Taylor, M. K.; Young, C. G. *Inorg. Chem.* **2012**, *51*, 3202.

(9) (a) Most, K.; Hoßbach, J.; Vidović, D.; Magull, J.; Mösch-Zanetti, N. C. *Adv. Synth. Catal.* **2005**, *347*, 463. (b) Lyashenko, G.; Saischek, G.; Judmaier, M. E.; Volpe, M.; Baumgartner, J.; Belaj, F.; Jancik, V.; Herbst-Irmer, R.; Mösch-Zanetti, N. C. *Dalton Trans.* **2009**, 5655. (c) Mayilmurugan, R.; Harum, B. N.; Volpe, M.; Sax, A. F.; Palaniandavar, M.; Mösch-Zanetti, N. C. *Chem.—Eur. J.* **2011**, *17*, 704.

(10) (a) Heinze, K.; Fischer, A. *Eur. J. Inorg. Chem.* **2007**, 1020. (b) Heinze, K.; Marano, G.; Fischer, A. *J. Inorg. Biochem.* **2008**, *102*, 1199. (c) Heinze, K.; Fischer, A. *Eur. J. Inorg. Chem.* **2010**, 1939. (d) Leppin, J.; Förster, C.; Heinze, K. *Inorg. Chem.* **2014**, *53*, 1039.

(11) Volpe, M.; Mösch-Zanetti, N. C. *Inorg. Chem.* **2012**, *51*, 1440.

(12) Hüttinger, K.; Förster, C.; Bund, T.; Hinderberger, D.; Heinze, K. *Inorg. Chem.* **2012**, *51*, 4180.

(13) Hüttinger, K.; Förster, C.; Heinze, K. *Chem. Commun.* **2014**, *50*, 4285.

(14) Rufanov, A.; Zarubin, D. N.; Ustynyuk, N. A.; Gourevitch, D. N.; Sundermeyer, J.; Churakov, A. V.; Howard, J. A. K. *Polyhedron* **2001**, *20*, 379.

(15) Holz, M.; Mao, X.; Seiferling, D.; Sacco, D. *J. Chem. Phys.* **1996**, *104*, 669.

(16) Stoll, S.; Schweiger, A. *J. Magn. Reson.* **2006**, *178*, 42.

(17) *SMART Data Collection and SAINT-Plus Data Processing Software for the SMART System* (various versions); Bruker Analytical X-Ray Instruments, Inc.: Madison, WI, 2000.

(18) Blessing, R. H. *Acta Crystallogr.* **1995**, *A51*, 33−38.

(19) Sheldrick, G. M. *SHELXTL*, version 5.1; Bruker AXS: Madison, WI, 1998.

(20) Sheldrick, G. M. *SHELXL-97*; University of Göttingen: Göttingen, Germany, 1997.

(21) Frisch, M. J.; Trucks, G. W.; Schlegel, H. B.; Scuseria, G. E.; Robb, M. A.; Cheeseman, J. R.; Scalmani, G.; Barone, V.; Mennucci, B.; Petersson, G. A.; Nakatsuji, H.; Caricato, M.; Li, X.; Hratchian, H. P.; Izmaylov, A. F.; Bloino, J.; Zheng, G.; Sonnenberg, J. L.; Hada, M.; Ehara, M.; Toyota, K.; Fukuda, R.; Hasegawa, J.; Ishida, M.; Nakajima, T.; Honda, Y.; Kitao, O.; Nakai, H.; Vreven, T.; Montgomery, J. A., Jr.; Peralta, J. E.; Ogliaro, F.; Bearpark, M.; Heyd, J. J.; Brothers, E.; Kudin, K. N.; Staroverov, V. N.; Kobayashi, R.; Normand, J.; Raghavachari, K.; Rendell, A.; Burant, J. C.; Iyengar, S. S.; Tomasi, J.; Cossi, M.; Rega, N.; Millam, J. M.; Klene, M.; Knox, J. E.; Cross, J. B.; Bakken, V.; Adamo, C.; Jaramillo, J.; Gomperts, R.; Stratmann, R. E.; Yazyev, O.; Austin, A. J.; Cammi, R.; Pomelli, C.; Ochterski, J. W.; Martin, R. L.; Morokuma, K.; Zakrzewski, V. G.; Voth, G. A.; Salvador, P.; Dannenberg, J. J.; Dapprich, S. Daniels, A. D.; Farkas, O.; Foresman, J. B.; Ortiz, J. V.; Cioslowski, J.; Fox, D. J. *Gaussian 09*, revision A.02; Gaussian, Inc.: Wallingford, CT, 2009.

(22) (a) Huzinaga, S.; Andzelm, J.; Klobukowski, M.; Radzio-Andzelm, E.; Sakai, Y.; Tatewaki, H. *Gaussian Basis Sets for Molecular Orbital Calculations*; Elsevier: Amsterdam, The Netherlands, 1984;. (b) Barone, V. In *Recent Advances in Density Functional Methods*; Chong, D. P., Ed.; World Scientific: Singapore, 1995; Part 1. (c) The WTBS basis set was obtained from the *Extensible Computational Chemistry Environment Basis Set Database*, version 02/02/06, as developed and distributed by the Molecular Science Computing Facility, Environmental and Molecular Sciences Laboratory, which is part of the Pacific Northwest Laboratory, P.O. Box 999, Richland, WA 99352, and funded by the U.S. Department of Energy. The Pacific Northwest Laboratory is a multiprogram laboratory operated by the Battelle Memorial Institute of the U.S. Department of Energy under Contract DE-AC06-76RLO..

(23) Mueller-Westerhoff, U. T.; Swiegers, G. F. *Synth. Commun.* **1994**, *24*, 1389.

(24) Broomfield, L. M.; Wright, J. A.; Bochmann, M. *Dalton Trans.* **2009**, 8269.

(25) The stereochemistry of the complexes under study will be described by the configuration index according to the Cahn−Ingold−Prelog system in an octahedral complex OC-6−*x*−*y* with the priority sequence used as follows: P > O > $N^{pyrrolato}$ > N^{imine}. The first index *x* refers to the ligand priority of the ligand trans to the ligand of the highest priority (axial ligands), and the second index *y* refers to the ligand priority trans to the ligand of the equatorial plane, which has the highest priority of these four equatorial ligands. Thus, Mo^{VI} complex ^{iPr2}**1** possesses OC-6−4−4 stereochemistry and Mo^{IV} complex ^{iPr2}**2** possesses OC-6−3−3 stereochemistry, as depicted in Schemes 2 and 3.

(26) (a) Cahn, R. S.; Ingold, C. K.; Prelog, V. *Angew. Chem., Int. Ed. Engl.* **1966**, *5*, 385. (b) Prelog, V.; Helmchen, G. *Angew. Chem., Int. Ed. Engl.* **1982**, *21*, 567. (c) Block, B. P.; Powell, W. H.; Fernelius, W. C.

Inorganic chemical nomenclature: principles and practice; ACS Professional Reference Book; American Chemical Society: Washington, DC, 1990. (d) von Zelewsky, A. *Stereochemistry of Coordination Compounds*; John Wiley & Sons Ltd., Chichester, U.K., 1996.
(27) Connelly, N. G.; Geiger, W. E. *Chem. Rev.* **1996**, *96*, 877.
(28) Tolman, C. A. *Chem. Rev.* **1977**, *77*, 313.
(29) Addison, A. W.; Rao, T. N.; Reedijk, J.; van Rijn, J.; Verschoor, G. C. *J. Chem. Soc., Dalton Trans.* **1984**, 1349.
(30) Lyashenko, G.; Herbst-Irmer, R.; Jancik, V.; Pal, A.; Mösch-Zanetti, N. C. *Inorg. Chem.* **2008**, *47*, 113.
(31) Saurenz, D.; Demirhan, F.; Richard, P.; Poli, R.; Sitzmann, H. *Eur. J. Inorg. Chem.* **2002**, 1415.
(32) Ricard, L.; Martin, C.; Wiest, R.; Weiss, R. *Inorg. Chem.* **1975**, *14*, 2300.
(33) Lim, B. S.; Willer, M. W.; Miao, M.; Holm, R. H. *J. Am. Chem. Soc.* **2001**, *123*, 8343.
(34) Dahlstrom, P. L.; Hyde, J. R.; Vella, P. A.; Zubieta, J. *Inorg. Chem.* **1982**, *21*, 927.
(35) Koch, W.; Holthausen, M. C. *A Chemist's Guide to Density Functional Theory*; Wiley-VCH: Weinheim, Germany, 2001.
(36) Bunker, M. J.; Green, M. L. H. *J. Chem. Soc., Dalton Trans.* **1981**, 847.
(37) Antczak, M. I.; Montchamp, J.-L. *Org. Lett.* **2007**, *10*, 977−980.
(38) (a) Klein, E. L.; Raitsimring, A. M.; Astashkin, A. V.; Rajapakshe, A.; Johnson-Winters, K.; Arnold, A. R.; Potapov, A.; Goldfarb, D.; Enemark, J. H. *Inorg. Chem.* **2012**, *51*, 1408. (b) Bray, R. C.; Lamy, M. T.; Gutteridge, S.; Wilkinson, T. *Biochem. J.* **1982**, *201*, 241.